University of South Bohemia in České Budějovice

Faculty of Science

Characterization of nuclear and cytoplasmic interactome of tick-borne encephalitis virus capsid protein

Master thesis

Bc. Kateřina Jaklová

Supervisor: RNDr. Martin Selinger, Ph.D.

Co-supervisor: RNDr. Pavlína Věchtová, Ph.D.

České Budějovice, 2023

Jaklová, K., 2023: Characterization of nuclear and cytoplasmic interactome of tick-borne encephalitis virus capsid protein. Mgr. Thesis, in English. – 59 p., Faculty of Science, University of South Bohemia, České Budějovice, Czech Republic.

Annotation

The aim of this work was to identify the interaction partners of the tick-borne encephalitis virus capsid protein within the cytoplasmic, membrane, and especially the nuclear fraction of infected DAOY HTB-186 cells. Firstly, the subcellular fractionation method was optimized. Secondly, the immunoprecipitation method and benzonase digestion were optimized; and finally, interaction partners from each fraction were identified using mass spectrometry.

Declaration

I declare that I am the author of this qualification thesis and that in writing it I have used only the sources and literature displayed in the list of used sources.

České Budějovice, 2023

…………………………………

Bc. Kateřina Jaklová

Acknowledgements

Content

1 Abstract

The tick-borne encephalitis virus (TBEV) is an arbovirus transmitted by ticks related to other well-known viruses (Dengue or Zika) that attacks the central nervous system and causes a disease called tick-borne encephalitis, whose incidence is steadily increasing in Europe and especially in the Czech Republic. As there is no specific therapy against TBEV infection, efforts have been made to find a potential candidate for drug design. One of these is a TBEV capsid (TBEV C) protein that is responsible for the formation of nucleocapsids and whose unexplained nuclear localization has been documented by our laboratory (Laboratory of Applied Biochemistry, FSc USB). The aim of this work was to identify the interaction partners of this viral protein and thereby understand more about its function in the nucleus. The results represent cytoplasmic, membrane, and nuclear interactomes of the TBEV capsid protein. This protein targeted histone (H2A and H2B) during the infection process as well as interacted with the NEB-specific glycolytic enzymes (Glyceraldehyde-3-phosphate dehydrogenase, Lactate dehydrogenase A, and Transketolase). These findings indicate an important role of the TBEV capsid protein in the nucleus. However, since comparison with the whole-cell TBEV capsid protein interactome presented by Selinger et al. (2022) showed differences and the mass spectrometry identification did not provide sufficiently relevant data for the overall evaluation, further research is needed to verify all these findings and to better understand the reason of the TBEV capsid protein localization to the nucleus and its functions in it.

2 Literature review

2.1 Flaviviruses

Flaviviruses are a group of small, single-stranded positive RNA viruses belonging to the family *Flaviviridae* with RNA genomes of 9 000-13 000 bases (Simmonds et al., 2017). This family includes arthropod-borne viruses (arboviruses) that are transmitted by ticks or mosquitoes (Gould & Solomon, 2008) and circulate worldwide. Many flaviviruses cause serious problems in both tropical and subtropical regions (Sotcheff & Routh, 2020), and as the human population grows and global warming occurs, their geographic distribution is increasing (Barrows et al., 2018). Most of these arboviruses are pathogenic, host-specific, and considered important veterinary and human pathogens due to their ability to infect vertebrates, especially humans or other mammals (Simmonds et al., 2017). Each year, hundreds of millions of human infections are caused by flaviviruses (le Breton et al., 2011), and since flaviviruses cause serious human diseases and can potentially contribute to long-term disability or even death, they constitute a major public health concern (Mazeaud et al., 2018).

2.1.1 Taxonomy

The *Flaviviridae* family consists of 4 genera (*Pestivirus*, *Hepacivirus*, *Flavivirus*, and *Pegivirus*) including more than 60 species (Simmonds et al., 2017). *Pestivirus* infections typically result in diseases with severe economic effects, such as classical swine fever or bovine viral diarrhea (Simmonds et al., 2017). These viruses mostly affect pigs or ruminants but can infect humans as well; however, in case of human infection, Pestiviruses have not been conclusively linked to any diseases (Simmonds et al., 2017). The hepatitis C virus, a human pathogen that causes liver disorders including cirrhosis or even cancer, is among the viruses in the *Hepacivirus* genus that can infect humans as well as rats, horses, bats, cows, or primates (Simmonds et al., 2017). The most important genus is *Flavivirus*, which contains many common arboviruses. The primary hosts are typically vertebrates, and the infection typically presents from an asymptomatic form to severe neurological sickness or haemorrhagic fever. This genus includes the highly studied dengue virus (DENV), Zika virus (ZIKV), tick-borne encephalitis virus (TBEV), and West Nile virus (WNV; Simmonds et al., 2017).

2.1.2 Phylogenetic relationships

The evolutionary relationships of flaviviruses are correlated with their epidemiology, biogeography, and disease associations. Flaviviruses are grouped into three classes according to how they spread – transmitted by ticks, mosquitoes, and viruses with no-known vectors (Fig. 1; Gaunt et al., 2001). For mosquito-borne flaviviruses, two distinct epidemiological groups (neurotropic and non-neurotropic) have been identified. Neurotropic viruses linked to the *Culex* species vector frequently cause encephalitic diseases. Contrarily, non-neurotropic viruses are linked to haemorrhagic disorders and the *Aedes* vector (Gaunt et al., 2001). Yellow fever virus, DENV, ZIKV, Japanese encephalitis virus (JEV), or WNV are examples of mosquito-borne viruses (Simmonds et al., 2017). Two groups of tick-borne flaviviruses exist – associated with seabirds and those related to rodents (Gaunt et al., 2001). Particularly among the tick-borne viruses are TBEV, Powassan virus (POWV), Louping-ill virus (LIV), Kyasanur forest disease virus (KFDV), and Omsk haemorrhagic fever virus (OHFV; Simmonds et al., 2017). No-known vector viruses are associated with bats (Gaunt et al., 2001).
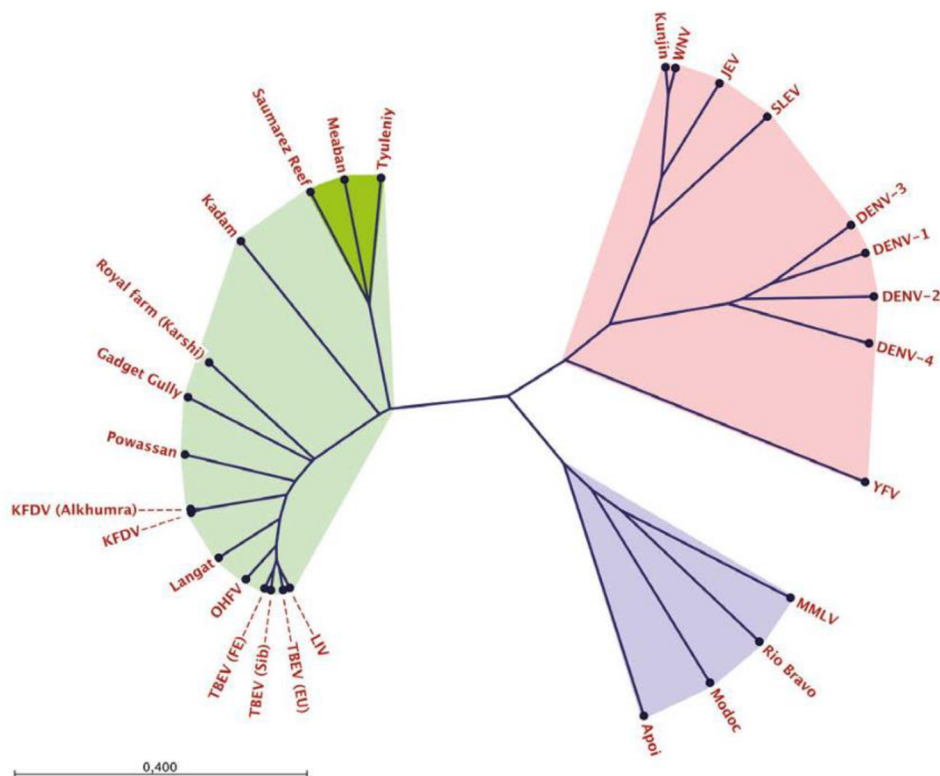

Figure 1: Maximum likelihood phylogenetic relationships of complete polyprotein sequences of representative individuals of flaviviruses. Light green colour – tick-borne flaviviruses, deep green colour – tick-borne seabirds flaviviruses, pink colour – mosquito-borne flaviviruses, violet colour – no-known vector flaviviruses (Valarcher et al., 2015).

Many aspects differentiate tick-borne flaviviruses from mosquito-borne ones. Mosquito-borne flaviviruses are transmitted horizontally and can spread to new areas, causing enormous epidemics. Oppositely, tick-borne flaviviruses usually occur only in certain regions and have a longer life cycle, which means that they need to be sustained in infected ticks for a long time (Lindqvist et al., 2018). Also, tick-borne viruses emerge at lower rates due to low virus replication and an extended tick generation cycle compared to a higher viral turnover in mosquitoes with a much faster life span (Dobler, 2010).

2.1.2.1 Members of mosquito-borne flaviviruses

The most prevalent flaviviruses spread by mosquitoes are DENV and ZIKV. DENV is characterized by widespread epidemics that have a substantial negative impact on human lives (Gubler, 1998). *Aedes* mosquitoes transmit DENV, which has been thoroughly investigated due to its infection with a wide spectrum of clinical manifestations ranging from febrile illness to fatal haemorrhagic disease (Gubler, 1998; Salles et al., 2018). This virus has 4 different serotypes (DENV1-4; Salles et al., 2018), and since DENV is a global pathogen (Colpitts et al., 2011), there are more than 350 million human cases reported every year (Bhatt et al., 2013). This number is increasing, although efforts have been made to stop its rapid spread (Bhatt et al., 2013). Major factors involved in the contemporary higher incidence of DENV are extraordinary population growth and uncontrolled urbanization. Also, a lack of effective mosquito control and increased air travel contribute to this issue (Gubler, 1998). Specific antivirals or vaccines against DENV are still not available, therefore, patients usually require a high-level expensive care (Colpitts et al., 2011).

ZIKV is another mosquito-borne virus transmitted to humans primarily by infected *A. aegypti* mosquitoes, although cases of human-to-human transmission through sexual intercourse and from mother to fetus during pregnancy have been recorded (Pielnaa et al., 2020). ZIKV infections are usually characterized by mild influenza-like symptoms, and severe cases may include Guillain-Barre syndrome (Plourde & Bloch, 2016). The rapid spread of ZIKV causes a serious global problem, especially in Latin American and Caribbean nations. There were between 44 000 to 1.3 million cases reported in Brazil during the 2016 epidemic (Pielnaa et al., 2020) that caused a rapid spread throughout the Americas. In addition, there is no effective treatment or a vaccine against ZIKV available, and many facts about ZIKV are still not solved at all, including its genetic diversity or the potential synergistic effects of co-infection with other viruses (Plourde & Bloch, 2016).

4

2.1.2.2 Members of tick-borne flaviviruses

As mentioned above, tick-borne flaviviruses cause serious diseases worldwide and, besides TBEV, include POWV, LIV, or KFDV.

POWV can be found in the Russian Far East (Kemenesi & Bányai, 2019) and is the only flavivirus representative of North America (especially the USA; Fig. 2), where almost 100 human cases were reported. There has been an increase in POWV infections during the past decade (Lindqvist et al., 2018). Despite the low incidence of POWV infection, 10-15 % of cases are fatal (Kemenesi & Bányai, 2019). The virus is transmitted to small mammals mainly by *Ixodes scapularis* and *I. cookei,* and milk-borne transmission has also been documented (Lindqvist et al., 2018). The symptoms of POWV infection similar as for other flaviviruses, including headache, fever, vomiting, or fatigue. In severe cases, memory problems also appear, and there are no available antiviral medications or vaccines against POWV (Lindqvist et al., 2018).
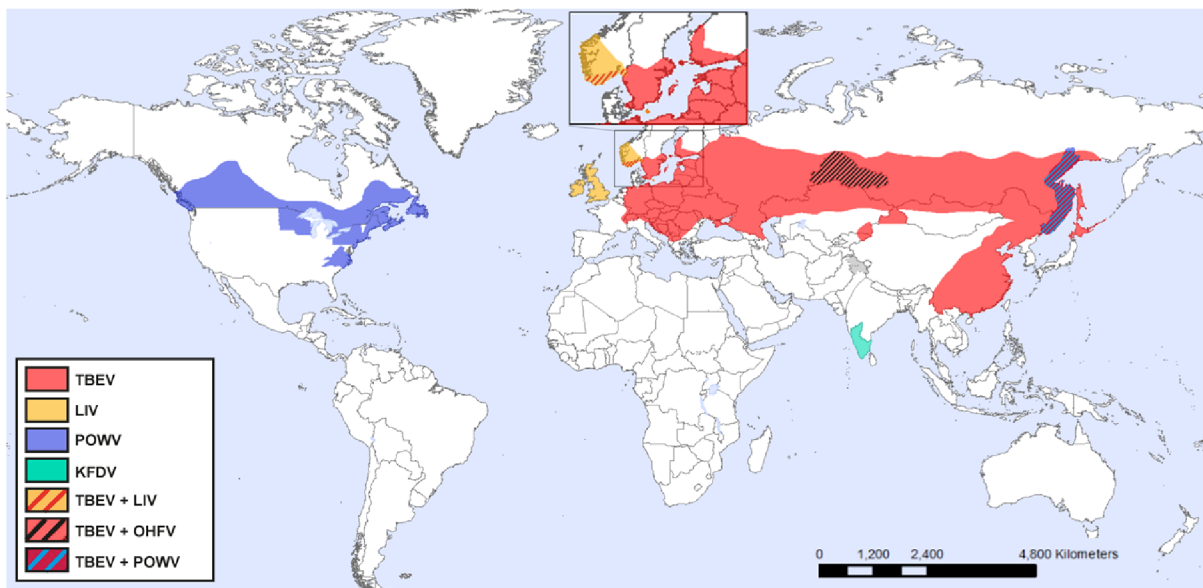
Figure 2: Distribution of TBEV, LIV, POWV, KFDV and OHFV. Red colour – TBEV regions. Yellow colour – LIV regions. Blue colour – POWV regions. Green colour – KFDV regions (Lindqvist et al., 2018).

LIV is distributed in areas of Great Britain and Ireland, but some cases have also occurred in Sweden or Denmark (Fig. 2; Lindqvist et al., 2018). It is transmitted by *I. ricinus* and usually causes a febrile disease in sheep that can progress to fatal encephalitis. 171 sheep cases were reported in Great Britain between 2012 and 2021 (Folly et al., 2022). Humans can also be infected (31 human cases were described between 1934 and 1991). LIV symptoms are

similar to influenza-like symptoms that can progress to severe neurological complications (Lindqvist et al., 2018).

KFDV causes Kyasanur forest disease (KFD; monkey fever), which is a haemorrhagic fever found especially in India (Fig. 2; Munivenkatappa et al., 2018), although a similar variant (Alkhurma haemorrhagic fever virus) has also been detected in Saudi Arabia. The symptoms are identical but may also include bleeding from the mouth, nose, or gastrointestinal tract. Ticks from the genus *Hemaphysalis* transmit the KFDV, and there are approximately 500 reported cases every year. Since there is no specific antiviral drug against KFDV, and existing vaccine is still not very effective, the number of KFD cases in India is increasing (Lindqvist et al., 2018).

2.2 TBEV

TBEV is a significant viral pathogen (Lindqvist et al., 2018) that affects humans and causes a central neural system (CNS) disease called tick-borne encephalitis (TBE). TBE was first described in Austria (Schneider, 1931) and TBEV was first isolated in Russia (Gould & Solomon, 2008). TBEV belongs to the TBEV serocomplex and the group of mammalian tick-borne viruses (Valarcher et al., 2015). This virus is widespread, particularly in Eurasia and the taiga forest areas (Kovalev & Mukhacheva, 2017), and an estimated 13 000 people contract the disease each year (Lindqvist et al., 2018). TBEV infection can have asymptomatic or symptomatic progress (meningitis, encephalitis, or meningoencephalitis) and often leads to life-long neurological complications or even death (Pulkkinen et al., 2018). At this moment, there is no specific therapy for TBEV available (Kaufman et al., 2020).

2.2.1 Subtypes

Three predominant subtypes of TBEV are present – European (TBEV-Eu), Siberian (TBEV-Sib), and Far Eastern (TBEV-FE; Valarcher et al., 2015). 14 species of ticks from the genus *Ixodes* were described as TBEV vectors (Valarcher et al., 2015). *I. ricinus* is primarily responsible for the transmission of the TBEV-Eu, which is common across western, northern, and eastern Europe as well as the European regions of Russia. According to Valarcher et al. (2015), the primary tick vector for the subtypes TBEV-Sib and TBEV-FE is *I. persulcatus*, and its geographic distribution spans from Japan to the Baltic states. There are also a few locations in China and Mongolia where the TBEV-FE subtype is present. There are three other phylogenetic lineages that are included in TBEV-Sib – South-Siberian, Baltic,

6

and Asian. Over the years, efforts have been made to reconsider the classification of TBEV, and a new Baikalian subtype (reviewed in Kovalev & Mukhacheva, 2017) and a Himalayan subtype discovered in the wild rodent *Marmota himalayana* in the Qinghai-Tibet Plateau in China (reviewed in Dai et al., 2018) were introduced. TBEV infection by any of the subtypes is a serious problem, but the most severe cases are observed with TBEV-FE infection due to its high rates of neurological complications, and up to 40 % of all cases are incurable (Pulkkinen et al., 2018). TBEV-Eu infection causes neurological problems in up to 10 % of patients (with a mortality rate of 0.5-2 %). Patients infected with TBEV-Sib typically experience protracted illnesses, and this subtype has a mortality rate of between 2 and 3 % (Pulkkinen et al., 2018).

2.2.2 Transmission

As previously established, TBEV can infect vertebrates, and all tick life stages of tick development (larvae, nymphs, adults) can spread the virus. Nymphs pose the highest challenge because of their enormous population. The major way that tick contract TBEV is by feeding on an infected host. Furthermore, TBEV transmission can be facilitated by co-feeding of uninfected tick adjacent to an infected tick on a non-infected host (Valarcher et al., 2015). Transmission from parent to offspring is also possible. This transovarial transmission is a persistent viral transmission that occurs when viral particles penetrate the ovaries. Humans can also be infected by the consumption of raw milk from infected sheep, goats, or cows (Valarcher et al., 2015). Transmission by transfusion and transplanted organs is also exceptionally possible (Orlíková et al., 2021). Person-to-person transmission has not yet been confirmed, only transmission from an infected mother to a fetus (CDC & DHCPP, n.d.).

2.2.3 TBE manifestation and pathology

The incubation period of TBE is asymptomatic and lasts between 7 and 14 days. Some cases with shorter incubation durations have been described, but only after milk-borne exposure (CDC & DHCPP, n.d.). TBEV infection symptoms can be monophasic or biphasic (Kubinski et al., 2020). The first stage is viraemic, with patients typically experiencing headaches, lethargy, or flu-like symptoms (Valarcher et al., 2015). Only 20-30 % of all patients progress to the second stage of illness, when TBEV spreads to the CNS (Mandl, 2005). This stage is marked by an abrupt rise in fever, headache, nausea, photophobia, and sometimes paresis, paralysis, or coma (Valarcher et al., 2015). Additionally, there is a link between TBE and neuropsychiatric long-term side effects, including depression or attention deficit

disorder (Valarcher et al., 2015). A chronic form of TBE has been described in patients infected with TBEV-Sib and TBEV-FE (Mandl, 2005). In general, after TBEV-FE infection, the symptoms are more fatal and the mortality rate is higher (5-20 %) than during TBEV-Eu infection (1-2 %; CDC & DHCPP, n.d.). Animals suffering from TBE generally have asymptomatic progress, and clinical signs are rarely observed (Valarcher et al., 2015).

TBEV enters the skin through the bite of an infected tick and is neuropathogenic in humans but typically does not manifest symptoms in its natural hosts. The initial replication of TBEV at the site of a tick bite takes place primarily in dendritic cells (Lindqvist et al., 2018) and Langerhans cells (Chambers & Diamond, 2003), which are crucial because they help the virus spread to the draining lymph nodes (Mandl, 2005). This leads to primary viremia and subsequent infection of peripheral tissues (Lindqvist et al., 2018). High levels of viremia are required for the secondary viremia. The mechanism by which the virus can infect the CNS by crossing the blood-brain barrier has not yet been clearly described (Mandl, 2005). Neurons are the initial targets of viral CNS invasion, while other types of cells may also become infected (Mandl, 2005).

2.2.4 Epidemiology

In total, there are more than 13 000 infected people with TBEV worldwide (Lindqvist et al., 2018), and 3 000 Europeans must be hospitalized each year (Valarcher et al., 2015). In general, TBE has been observed in 28 countries, and especially Baltic states and Russia are countries with the highest incidence of TBE (Valarcher et al., 2015). Due to climate changes, TBE is spreading to western and northern regions and to higher altitudes (Orlíková et al., 2021). The Czech Republic is one of the countries with a higher incidence as well. In 2020, a total of 854 cases (503 males and 351 females) were reported, and the incidence has increased during the past five years from 3.37 to 7.98 cases per 100 000 inhabitants (Orlíková et al., 2021). 90.9 % of these cases required hospitalization and 60.5 % of these cases were hospitalized at infectious disease departments. A total of 5 patients succumbed to the TBEV infection due to severe complications. However, the death rate in 2020 is comparable to the situation in previous years (Orlíková et al., 2021).

Since there is no available therapy, TBEV infection can only be prevented by active immunization (Kaufman et al., 2020). All individuals at risk of exposure to the pathogen should receive an inactivated TBE vaccination (Orlíková et al., 2021). Based on the K23 isolate (Encepur) and the Neudoerfl isolate (FSME-IMMUN), there are two vaccinations (both TBEV-Eu subtypes) that are readily available in Europe (Kollaritsch et al., 2012;

Kubinski et al., 2020). Other vaccines include the 205 (EnceVir) and the TBEV-FE Sofjin isolates (Moscow, Tick-E-Vac, and Klesch-E-Vac) used in Russia (Kollaritsch et al., 2012; Kubinski et al., 2020). A Chinese vaccine, SenTaiBao, based on the Chinese TBEV-FE Sen-Zhang isolate, is another possible alternative, especially in Asia (Kubinski et al., 2020; Xing et al., 2017). The basic vaccination strategy consists of 3 doses, and the first revaccination occurs after three years. Following that, revaccination is needed once in five years (Orlíková et al., 2021).

2.3 TBEV molecular and genetic characteristics

Mature virions of TBEV are about 50 nm in diameter and consist of electron-dense nucleocapsid surrounded by lipid membrane derived from the host cell. The nucleocapsid is formed by capsid protein (C) and the genomic ssRNA (Fig. 3). Two glycoproteins, envelope (E) and membrane (M), are incorporated into the lipid bilayer via their transmembrane domains (Kemenesi & Bányai, 2019). The E protein is the main surface protein that interacts with cell receptors and mediates fusion of viral and cell membranes (Gritsun et al., 2003). The M protein has two functional forms. In the internal (immature) virions, glycosylated precursor M (prM) stabilizes the E protein (Kemenesi & Bányai, 2019), and the cleavage of prM to M occurs when the virions leave the cell (Gritsun et al., 2003).
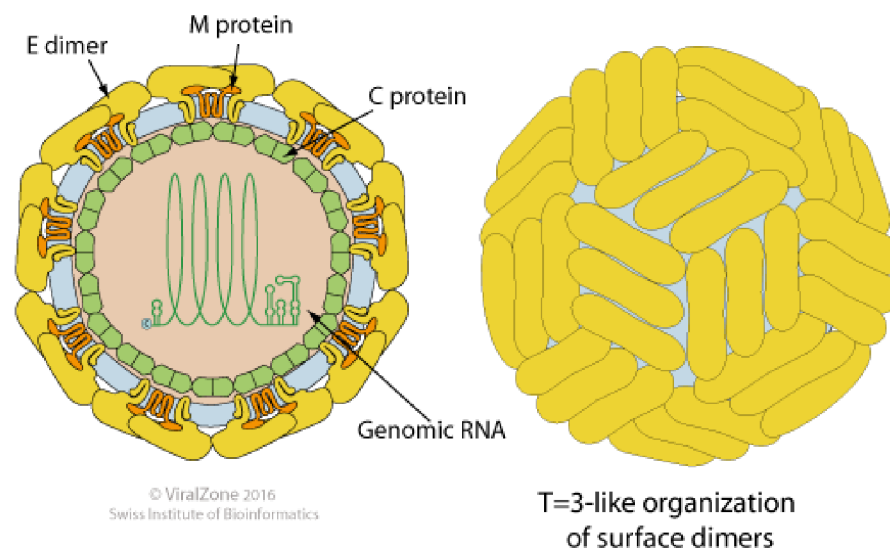
Figure 3: TBEV virion structure. Yellow colour – E dimer. Orange colour – M protein. Green colour – C protein with the genomic RNA (*Flaviviridae ~ ViralZone*, n.d.).

The TBEV genome is approximately 11 kb in size, and TBEV genomic RNA contains one open reading frame (ORF) encoding a single polyprotein with a length of about 3 400 amino acids. The ORF is flanked by 5´ and 3´ non-coding regions (NCR) containing highly stable secondary structures necessary for viral replication (Fig. 4; Kemenesi & Bányai, 2019). Viral and cellular proteases split the translated polyprotein into the three structural proteins (C, E, and prM/M) and seven non-structural proteins (NS1, NS2A, NS2B, NS3, NS4A, NS4B, and NS5; Gritsun et al., 2003). The 5' NCR of the genomic RNA is approximately 130 nucleotides long, in contrast with the 3' NCR that is 400-700 nucleotides long and is composed of a stable stem-loop structure (Kemenesi & Bányai, 2019).
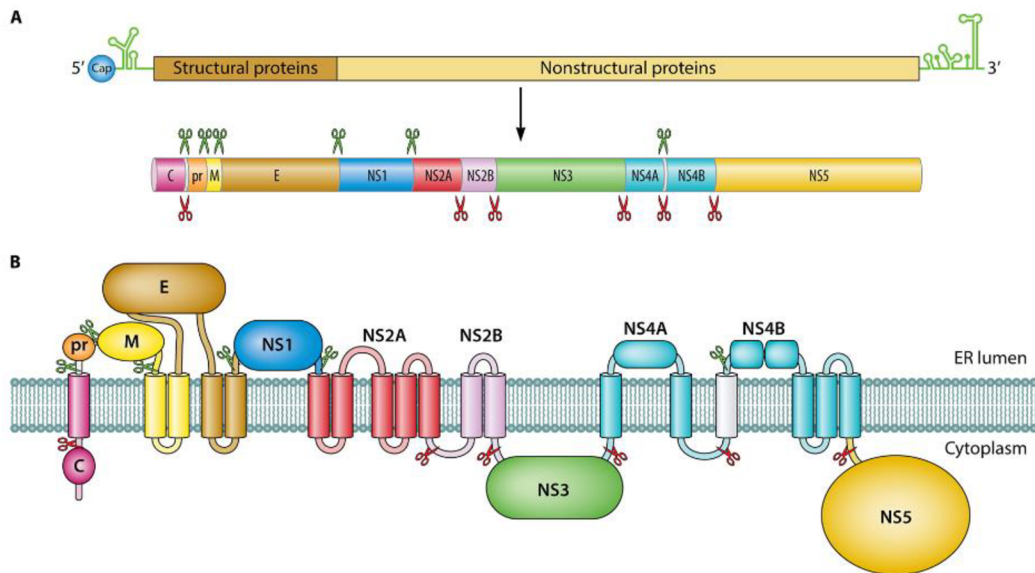
Figure 4: A – schematic TBEV genome organization and translation of the viral polyprotein. B – proteolytic cleavage sites, individual proteins, and their localization (Kemenesi & Bányai, 2019).

The 3´part of ORF encodes the non-structural proteins mentioned above. NS1 protein exists in a variety of shapes and is connected to membranes. Virus-specific serine protease activity is provided by the NS3 protein in complex with the NS2B protein (Gritsun et al., 2003). The NS3 serine protease activity is crucial for cleaving the viral polyprotein, while its RNA triphosphatase and RNA helicase activities are involved in viral RNA synthesis and capping (Kemenesi & Bányai, 2019). The NS4A and NS4B proteins are crucial for polyprotein orientation within intracellular membranes (Gritsun et al., 2003). The NS5 protein bears a methyltransferase domain and RNA-dependent RNA polymerase domain and is responsible for viral genome replication (Kemenesi & Bányai, 2019).

10

2.3.1 TBEV replication cycle

The TBEV replication cycle is intricate and includes numerous steps (Fig. 5). The virus enters the host cell through the endocytic pathway after interacting with surface receptors. In mammalian cells, there are two receptor candidates – laminin-binding protein and $\alpha V\beta 3$ integrin (Pulkkinen et al., 2018). Also, heparan sulfate has been identified as one of the possible TBEV receptors (Kemenesi & Bányai, 2019). The viral and endosomal membranes fuse due to low pH in the late endosome, allowing the virus to uncoat and enter the cytoplasm. The ribosomes of the rough endoplasmic reticulum (ER), where the replication of the viral RNA takes place, are responsible for the production of viral proteins. Genome replication occurs directly in virus-induced invaginations of the ER, and newly synthesized genomes are captured by the C protein on the ER cytoplasmic side. The nucleocapsid complex acquires its membrane-embedded E and M proteins by budding through the membrane into the ER lumen. The immature particles travel through the Golgi network and mature in the acidic *trans*-Golgi environment. Along with mature particles, immature particles are also released from the cell. Fully developed particles can start a new round of infection; the immature particles cannot fuse and are regarded as non-infectious (Pulkkinen et al., 2018).

Figure 5: TBEV replication cycle including receptor binding, entry, fusion, protein synthesis, replication in ER, assembly and budding into ER, transport through Golgi complex, maturation, and egress (Pulkkinen et al., 2018).

2.4 TBEV C

The TBEV C protein (~ 11 kDa) is the smallest structural protein found in flaviviruses and contains approximately 100 amino acid residues (Kaufman et al., 2020). The homology o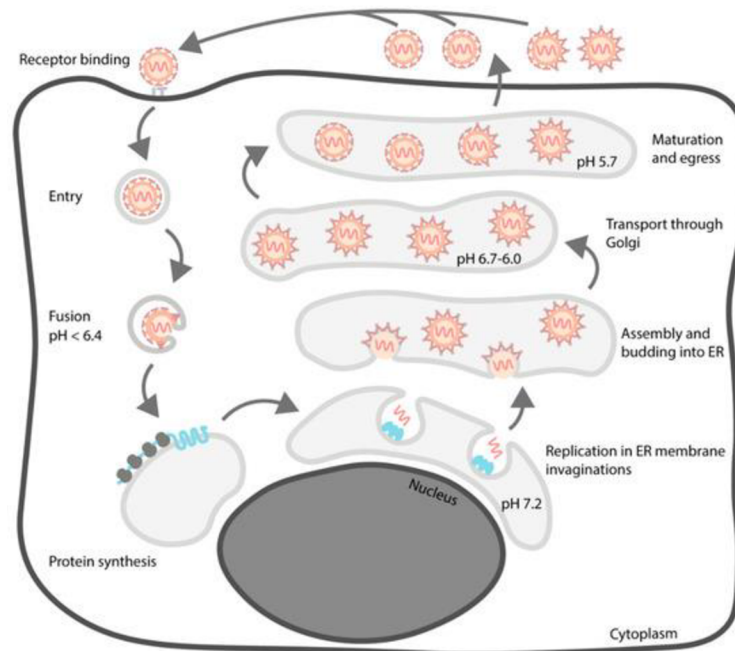f TBEV C amino acids is the lowest among flaviviruses as it shares only 25 % of its amino acid sequences with, for instance, JEV C (Zhang et al., 2021). However, the *Flaviviridae* C proteins exhibit significant biochemical traits and structural features that are well preserved and contribute to overlapping C activities (Zhang et al., 2021). TBEV C is found at the N-terminus and is synthesized first during translation (Kofler et al., 2002). This protein has a significant positive charge due to high number of basic amino acids. As a result of this property, TBEV C is considered a member of supercharged proteins (Kaufman et al., 2020).

2.4.1 TBEV C structure

The general flavivirus C structure (Fig. 6) was described in Zhang et al. (2021) and Roby et al. (2015) articles. WNV C and DENV C structures were solved by nuclear magnetic resonance (NMR) or X-ray crystallography (Dokland et al., 2004; Ma et al., 2004). There are two highly conserved inner regions in each C protein molecule (hydrophobic and cationic). The C protein was discovered to be primarily a dimer, containing in its structure two α-helical conformations with four α-helices (α1 – α4) linked by short loops, which are crucial for viral assembly and stability. The α1 helix, present in the central hydrophobic area, is important for interactions with viral surface proteins. The longest helix, known as helix α4, is found near the hydrophobic C-terminal end. The assembly of nucleocapsids and viruses depends on the α4–α4′ interaction (Zhang et al., 2021). Additionally, the α4 and α4′ helices are considered responsible for nonspecific electrostatic interactions with viral RNA (Kaufman et al., 2020). The α1–α1′ and α2–α2′ helices are located on the opposite sides of the α4-α4′ helix. The α3–α3′ helix is parallel to the α4–α4′ helix, and the α1 and α3 helices are amphipathic and mainly contain leucine residues (Zhang et al., 2021).

The first 3D structure of TBEV C protein was described by Selinger et al. (2022) using high-resolution NMR spectroscopy in combination with arithmetical methods (Fig. 6). The Δ16-TBEV C contains 4 α-helices and forms both monomers and homodimers. However, a comparison of the Δ16-TBEV C NMR structure with previously solved 3D structures of other flaviviral C proteins showed similarities but also some minor differences. The main difference is that the unstructured part of the N-terminal part of TBEV C is shorter (by 7–17 amino acids), and all helices in Δ16-TBEV C are sequentially shifted by more than 6 amino acids to the N-terminal end (Selinger et al., 2022).
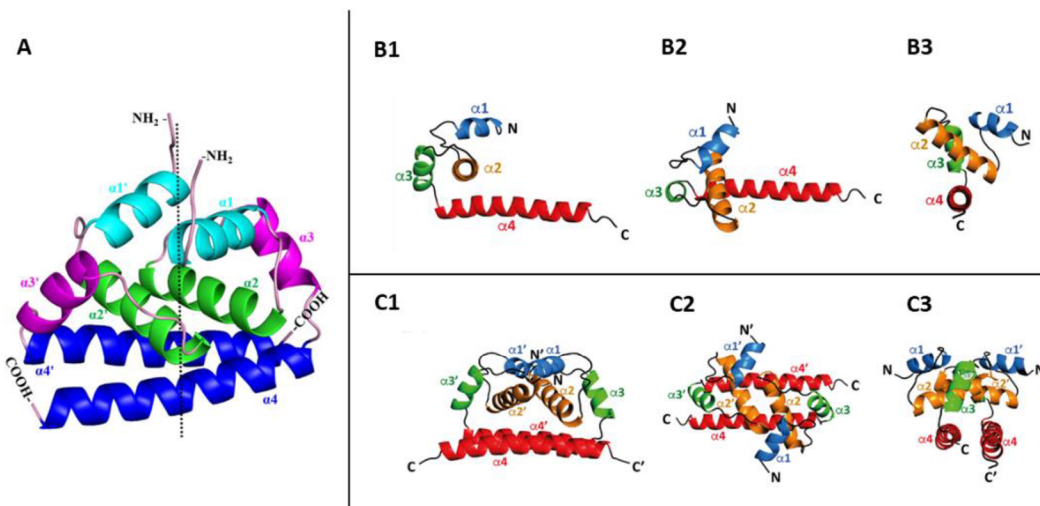
Figure 6: 3D structures of: A – flaviviral C (Zhang et al., 2021). B – monomeric Δ16-TBEV C, C –homodimer Δ16-TBEV C. 1 – TBEV C side view. B2 – TBEV C top view. B3 – TBEV C front view (Selinger et al., 2022).

2.4.2 TBEV C function and localization

TBEV C has multiple functions, but the most crucial is the formation of nucleocapsids and its role in promoting the proper assembly of infectious particles (Kemenesi & Bányai, 2019). TBEV C is also bound to viral RNA and has other cell regulation functions in infected cells. This protein may affect how host proteins are expressed and interfere with the immune system. Additionally, it is linked to several cell proteins that contribute to the pathogenesis of viruses (Zhang et al., 2021). Many C proteins have been used as a target for antivirals in other virus families (such as retroviruses, etc.), and therefore TBEV C can be a possible candidate for the drug design within flaviviruses (Sotcheff & Routh, 2020).

The localization of TBEV C is mainly cytoplasmic since the assembly of TBEV takes place mainly in the ER. However, TBEV C was also detected on the surface of lipid droplets and in the nuclei (nucleoli) of infected cells (Selinger et al., 2022). Nuclear localization signals (NLSs) are basic amino acid sequences found in TBEV C, primarily arginine and lysine. These NLSs can interact with proteins that are part of nuclear import receptors, such as importin α/β. TBEV C nuclear (nucleolar) localization may play a significant role in how the virus interacts with the environment of the host; however, only a few details about the role of TBEV C in the nucleus have been clarified. In some previous studies dealing with other flaviviral C proteins (DENV C, JEV C, ZIKV C, and WNV C) an interference with ribosome biogenesis or apoptosis induction by activating the p53 signalling cascade was suggested (Selinger et al., 2022).

3 Aims and objectives

The main aim of this master thesis is the identification of the TBEV C interaction partners in the nuclear (nucleus) and cytoplasmic fraction of infected cells.

Other sub-goals are:

- optimization of cytoplasmic and nuclear fraction isolation of infected cells using subcellular fractionation (SF) methods
- optimization of immunoprecipitation using TBEV C specific antibodies and benzonase
- co-immunoprecipitation of TBEV C and its binding partners and their identification using mass spectrometry (MS)

4 Material and methods

4.1 Infection of DAOY HTB-186 and A549 cells

A stable human medulloblastoma cell line, DAOY (ATCC HTB-186), arising from a cerebellar medulloblastoma of a 4-year-old boy (Jacobsen et al., 1985), was used in all experiments. These cells were maintained by regular passages according to the instructions in DMEM medium (DMEM Low Glucose, Biosera), which also contained 10 % fetal bovine serum (BOFES), 1 % antibiotics and antimycotics (Amphotericin B 0.25 μg/ml, Penicillin G 100 units/ml, Streptomycin 100 μg/ml), and 1 % glutamine. DAOY cells were cultured at 37 °C and in 5 % CO_2 atmosphere. In addition, for TBEV C detection experiments, both DAOY cells and an adenocarcinoma human alveolar basal epithelial A549 cells (ATCC), were used. This cell line was created by removing and cultivating lung tissue from an explanted tumor belonging to a 58-year-old Caucasian man (Giard et al., 1973). The maintenance of these cells was the same as for DAOY cell line.

According to the type of experiment, cells were first seeded one day (24 hours) prior the infection. The number of cells in the samples was counted using a Bürker chamber and calculated using the formula: c = A × 2 × 10 000 [cells/ml], where c is the concentration of cells in 1 ml of suspension and A is the counted number of cells. A schematic cell density information is included in the Tab. I.

Table I: Seeding density and total volumes for 6-well plates and 25 cm² flasks.

Panel format	Experiment	Cell density	Total volume [ml]
6-well plate	Optimization	0.5×10^6	2
25 cm² flask	MS preparation	2×10^6	8

Infection was performed the following day. All work with infectious material was done in biosafety level 2 (BSL2) laboratories at the FSc USB. The highly pathogenic TBEV-Eu isolate Hypr (4th passage in suckling mouse brains, GenBank accession No. U39292) was used for infection. A brain suspension from uninfected mice was then used as a negative control. Conditions used during the whole infection process are shown in Tab. II and the volume of virus suspension was calculated according to the equation below:

$$\frac{multiplicity\ of\ infection\ (MOI)\ \times cell\ count}{viral\ suspension\ titer\ [PFU/ml]} = volume\ of\ viral\ suspension\ [ml]$$

Table II: Conditions for the infection of cell lines.

Experiment	Cell density	MOI	Concentration [PFU/ml]	Viral suspension volume [µl]	Total volume [ml]
Optimization	0.5×10^6	5	2.08×10^8	12.01	1
MS preparation	2×10^6	5	3.54×10^8	28.24	2.5

After 2 hours post infection (hpi), the viral suspension was removed and the cells were washed in phosphate-buffered saline (PBS; 2.72 g $Na_2HPO_4 \cdot 7 H_2O$, 8 g NaCl, 0.2 g KCl, 0.2 g KH_2PO_4, pH 7.4) and then fresh complete medium was added. Sampling was performed 24 or 36 hours after infection.

4.2 Rapid isolation of nuclei from cells *in vitro*

Rapid isolation of nuclei from cells *in vitro* (Nabbi & Riabowol, 2015) was performed using a modified protocol that demonstrates an efficient way to separate nuclei from cultured cells while causing as little protein degradation and contamination as possible. This method consisted of gradual separation of whole-cell lysate, cytoplasmic lysate, and nuclear fraction lysate, with subsequent verification of the purity of individual fractions by SDS-polyacrylamide gel electrophoresis (SDS-PAGE) and western blot (WB) using fraction-specific markers.

The culture medium was aspirated, and cells were washed with ice-cold PBS. Then, the cells were released using trypsinization, incubated for 3-5 minutes, and resuspended in 0.5 ml of complete culture medium. After resuspension, the cell suspension was transferred into a 1.5 ml microtube and centrifuged at 200 × g for 7 minutes at 4 °C. After that, cells were washed with ice-cold PBS once again. The supernatant was removed by aspiration, and the cell pellet was resuspended in 500 µl of washing buffer (ice-cold PBS containing 0.1% NP-40, non-ionic detergent) and protease inhibitors (Halt™ Protease Inhibitor Cocktail, Thermo Fisher Scientific, cat. No. 87786). The cell suspension was resuspended five times on ice, and 50 µl of the lysed cell suspension (whole-cell lysate) was transferred to a new tube and kept on ice in all the following steps until sonication. The remaining cell lysate (450 µl) was shortly centrifuged at 10 000 × g. The supernatant (cytoplasmic lysate) was then transferred to a new tube and kept on ice until the sonication step as well. The pellet was resuspended in 500 µl of washing buffer and shortly centrifuged at 10 000 × g. Then, the supernatant was discarded, and the pellet was resuspended in 100 µl of washing buffer

(this was the nuclear fraction lysate). After the isolation steps, all lysates were briefly sonicated (20 kHz, 2 pulses, 8 seconds) while on ice and further stored at -20 °C until use.

4.3 NE-PER nuclear and cytoplasmic extraction

Thermo Fisher Scientific NE-PER™ Nuclear and Cytoplasmic Extraction Reagents Kit (cat. No. 78833) was used for the preparation and separation of cytoplasmic and nuclear extracts from mammalian DAOY cells. The purity of individual fractions was later verified using the same methods as in the case of fractions from Chapt. 4.2.

All centrifugation steps were performed at 4 °C and all samples were kept on ice. At the very beginning, cells were harvested with trypsin, transferred to a 1.5 ml microtube, and centrifuged at 500 × g for 5 minutes. Following that, cells were resuspended in PBS and the tube was centrifuged at 500 × g for 2-3 minutes. The supernatant was carefully removed, leaving the cell pellet as dry as possible. Ice-cold cytoplasmic extraction reagent I (CER I) containing protease inhibitors (Halt™ Protease Inhibitor Cocktail) was added to the pellet, causing selective permeabilization of the cell membrane and release of cytoplasmic contents. Individual reagents volumes for 0.5×10^6 cells are in Tab. III.

Table III: Reagent volumes for 0.5×10^6 cells.

Cell density	CER I [μl]	CER II [μl]	NER [μl]
0.5×10^6	100	5.5	50

After adding CER I, the tube was vortexed at the highest speed for 15 seconds to fully resuspend the cell pellet and incubated on ice for 10 minutes. Then, ice-cold cytoplasmic extraction reagent II (CER II) containing protease inhibitors was added the tube and vortexed for 5 seconds at the highest speed. Then, the samples were incubated on ice for 1 minute, vortexed for 5 seconds at the highest speed, and centrifuged at maximum speed (~ 16 000 × g) for 5 minutes. Immediately following the centrifugation step, the supernatant (cytoplasmic extract) was transferred to a pre-chilled microtube and placed on ice until storage.

The insoluble (pellet) fraction containing nuclei was resuspended in ice-cold nuclear extraction reagent (NER) with protease inhibitors, vortexed at the highest speed for 15 seconds, placed on ice, and vortexed every 10 minutes for a total of 40 minutes. After incubation, the tube was centrifuged for 10 minutes at maximum speed (~ 16 000 × g) and the supernatant (nuclear extract) was transferred to a pre-chilled tube. Nuclear and cytoplasmic extracts were then stored at -80 °C until use.

4.4 Subcellular protein fractionation (SF)

Thermo Fisher Scientific Subcellular Protein Fractionation Kit for Cultured Cells (cat. No. 78840) was used for the preparation of cytoplasmic, membrane, nuclear soluble, chromatin-bound, and cytoskeletal protein extracts from mammalian cultured cells (DAOY and A549). The purity of individual fractions was verified using the same methods as mentioned in Chapts. 4.2 and 4.3. This kit was also used for the preparation of cytoplasmic, membrane, and nuclear fractions for subsequent identification using MS.

The first part of the SF process was similar to the NE-PER nuclear and cytoplasmic extraction. All centrifugation steps were performed at 4 °C and all samples were kept on ice. Cells (DAOY or A549) were harvested with trypsin, transferred to a 1.5 ml microtube, and centrifuged at 300 × g for 5 minutes. After that, the cells were washed in PBS. Then, the supernatant was carefully removed and discarded, leaving the cell pellet as dry as possible.

Firstly, ice-cold cytoplasmic extraction buffer (CEB) was added to the pellet and the tube was incubated at 4 °C for 10 minutes with gentle mixing. This buffer caused selective cell membrane permeabilization and released the soluble cytoplasmic contents. All reagents contained protease inhibitors (Halt^{TM} Protease Inhibitor Cocktail). Volumes of individual reagents for various cell counts are shown in Tab. IV.

Table IV: Reagent volumes for different cell amounts.

Experiment	Cell density	CEB [μl]	MEB [μl]	NEB [μl]	NEB+ [μl]	PEB [μl]
Optimization	0.5×10^6	100	100	50	50	50
MS preparation	2×10^6	200	200	100	100	100

After the incubation, the tube was centrifuged at 500 × g for 5 minutes, and the supernatant (cytoplasmic extract) was immediately transferred to a pre-chilled microtube and kept on ice until use or storage. Ice-cold membrane extraction buffer (MEB) containing protease inhibitors was added to the pellet, the tube was vortexed for 5 seconds at the highest speed and incubated at 4 °C for 10 minutes with gentle mixing. This reagent dissolved plasma, mitochondria, and ER/Golgi membranes, and after 10 minutes, the tube was centrifuged at 3 000 × g for 5 minutes. Membrane extract (supernatant) was transferred to a pre-chilled microtube and kept on ice.

Ice-cold nuclear extraction buffer (NEB) was added to the pellet as a third reagent that yielded the soluble nuclear extract. This buffer also contained protease inhibitors, and it was vortexed at the highest speed for 15 seconds and incubated at 4 °C for 30 minutes with gentle mixing. In the meantime, chromatin-bound extraction buffer (NEB+) containing protease inhibitors was prepared by adding 5 μl of 100 mM $CaCl_2$ and 3 μl of Micrococcal Nuclease (300 units) per 100 μl of room temperature NEB. After 30 minutes of incubation, the tube was centrifuged at 5 000 × g for 5 minutes and the supernatant (soluble nuclear fraction) was transferred to a pre-chilled tube on ice. Immediately after that, the prepared room temperature NEB+ was added to the pellet, the tube was vortexed at the highest speed for 15 seconds and incubated at room temperature for 15 minutes. Then, the tube was vortexed for another 15 seconds at the highest speed and the tube was centrifuged at maximum speed (~ 16 000 × g) for 5 minutes. The supernatant (chromatin-bound nuclear extract) was then transferred to a new tube and kept on ice.

Finally, room temperature pellet extraction buffer (PEB) containing protease inhibitors was added to the pellet, vortexed at the highest speed for 15 seconds, incubated at room temperature for 10 minutes, and centrifuged at maximum speed (~ 16 000 × g) for 5 minutes to isolate cytoskeletal proteins. The supernatant (cytoskeletal extract) was transferred to a new tube, and all samples were prepared for usage or storage at -80 °C.

4.5 Assessment of protein concentration using BCA assay

The assessment of protein concentration in all samples was performed using BCA Protein Assay Kit (Pierce, Thermo Fisher Scientific, cat. No. 23225). 2 μl of each sample obtained by SF methods and 8 μl of dH_2O was added to 200 μl of the reagent mixture, which was prepared according to the manufacturer's instructions in a ratio of 50:1 (v/v; buffers A:B). To construct the calibration curve, BSA standards of known concentrations were used, to which the mixture was also added in the same reagents volume. After incubation at 37 °C for 30 minutes, the absorbance at a wavelength of 562 nm was measured and a calibration curve was constructed. In the end, the exact concentration of individual samples was calculated, which was further used for the preparation of samples for the SDS-PAGE.

4.6 SDS-polyacrylamide gel electrophoresis (SDS-PAGE)

The SDS-PAGE method was used to separate proteins according to their size and was carried out in 12/15 % polyacrylamide gels depending on the target protein size. The separation gel was prepared based on the volumes listed in Tab. V. 2,2,2-trichloroethanol (TCE) was incorporated into gels, providing subsequent fluorescent visible detection of proteins without staining (stain-free detection).

Table V: Reagents volumes used for preparation of a 12/15 % (2nd/3rd column) gels.

Reagent	Volume [ml]	Volume [ml]
30 % AA (Rotiphorese® Gel 30; 37; 5:1)	2	2.5
4× separation buffer (1.5 M Tris-HCl; pH 8.8; 0.4 % SDS)	1.25	1.25
ddH$_2$O	1.7	1.2
10 % Ammonium Peroxodisulfate (APS; Lach:ner, #7727-54-0)	0.05	0.05
N,N,N',N'-tetramethylethylenediamine (TEMED)	0.002	0.002
2,2,2-trichloroethanol (TCE)	0.025	0.025

Immediately after mixing, the solution for the separation gel was poured between the glasses. To obtain a horizontal layer of the gel, the mixture was overlaid with 30 % isopropanol (v/v). After solidification, isopropanol was removed, the gel was washed, and the remaining water was carefully dried with filter paper. Then, a 5 % stacking gel (Tab. VI) with the required number of wells (10/15) was prepared.

Table VI: Reagents volumes used for preparation of a 5 % stacking gel.

Reagent	Volume [µl]
30 % AA (Rotiphorese® Gel 30; 37; 5:1)	165
4× stacking buffer (1.0 M Tris-HCl; pH 6.8; 0.4 % SDS)	250
ddH$_2$O	575
10 % APS (Lach:ner, #7727-54-0)	10
TEMED	1
TCE	5

During the solidification of the stacking gel, the samples were prepared. The needed volume of each sample containing 4 000 ng of proteins was calculated according to the concentration obtained by the BCA assay (Chapt. 4.5). Water was added to a total volume of 16 µl and also 4× loading buffer (LB) with dithiothreitol (DTT; 0.313 M Tris-HCl; pH 6.8; 10 % SDS; 50 % glycerol; 0.05 % bromophenol blue; 50 mM dithiothreitol). After the stacking gel solidified, the gels were placed in the electrophoretic apparatus, which was filled with 1× running buffer (0.025 M Tris; 0.192 M glycine; 0.1 % SDS) and samples (15 µl per well) were pipetted into the individual well. As a size standard, Protein Marker VI (10-245) prestained (AppliChem, cat. No. A8889) was used and electrophoretic separation lasted for 90 minutes at 100 V. After the separation, the gels were removed from the apparatus, washed with distilled water, and the protein profile was recorded by photo documentation of the TCE fluorescence signal excited by UV light (GENESys, V1.5.2.0). The documented gels were subsequently used for WB, and after its completion, the proteins were stained using PageBlue Protein Staining Solution (Thermo Fisher Scientific, cat. No. 24620).

4.7 Western blot (WB) and immunodetection

WB is a method used for the detection of proteins that are transferred to a PVDF (polyvinylidene difluoride) membrane. After completing the SDS-PAGE, PVDF membranes were first activated by incubation for 3-5 minutes in 100 % methanol, and blotting papers were placed in blotting buffer (0.025 M Tris-HCl; 0.192 M glycine; 20 % methanol). After incubation, we prepared a "blotting sandwich" (Fig. 7) that was assembled in a blotting apparatus (Trans-Blot® Turbo™ Transfer System, Bio-Rad). The transfer took 30 minutes at 20 V and 1 A as the maximum current.
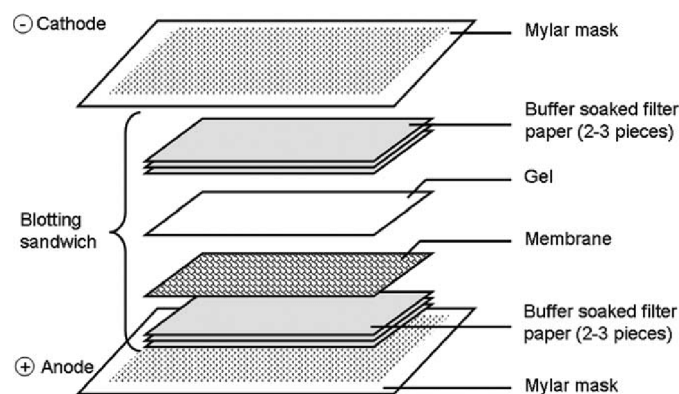
Figure 7: General scheme for the preparation of the "blotting sandwich" (Stewart & Veenstra, 2008).

Membranes with bound proteins were then blocked for 1 h at room temperature in a blocking solution of 5 % skimmed dry milk in PBS-T (PBS; 0.05 % Tween) or 3 % BSA (Roti® Albumin Fraction V) in PBS-T. Detection of the target protein was performed by incubating the membranes with primary antibodies (Tab. VII) diluted in blocking solution overnight at 4 °C. Secondary antibodies (Tab. VII) conjugated with horseradish peroxidase (HRP) were then used to detect the bound primary antibodies for the subsequent chemiluminescent detection. Membranes were always incubated with secondary antibodies for 1 hour at room temperature, and before adding them and after incubation, the membranes were washed 3× in PBS-T. For the detection of bound HRP-conjugated secondary antibodies, the WesternBright™ Quantum Kit (Advansta, cat. No. K-12042-D20) was used according to the manufacturer's instructions (mixing solutions A and B in a 1:1 ratio).

Table VII: List of used antibodies.

Antibody	Producer	Type	Experiment	Ratio
Anti-TBEV C	FSc USB	Primary	Optimization	1:1500
			MS preparation	1:1500
Anti-KDM1/LSD1	Abcam (cat. No. ab90966)	Primary	Optimization	1:500
Anti-beta III Tubulin	Abcam (cat. No. ab18207)	Primary	Optimization	1:500
Anti-Vimentin	Abcam (cat. No. ab188499)	Primary	Optimization	1:500
Anti-Guinea pig (HRP)	Invitrogen (cat. No. A16130)	Secondary	Optimization	1:1000
			MS preparation	1:1000
Anti-Mouse (HRP)	VectorLabs (cat. No. PI-2000)	Secondary	Optimization	1:1000
Anti-Rabbit (HRP)	VectorLabs (cat. No. PI-1000)	Secondary	Optimization	1:1000

4.8 Benzonase treatment

Benzonase was used to treat lysates prior to the immunoprecipitation method. This non-specific DNase and RNase was used to ensure the degradation of all DNA and RNA in samples, thereby eliminating the identification of false-positive nucleic acid-mediated binding partners. Firstly, the method was optimised using two sets of samples. The first set served as a negative control and contained SF lysates (CEB, MEB, NEB) and total RNA isolated from DAOY cells in an amount of 2 μg (provided by Dr. Martin Selinger). The second set was prepared the same way and contained extra benzonase (Benzonase® Nuclease, ≥250 units/μl, Merck, cat. No. E1014), and for complete degradation, it was also required to add 2 mM MgCl$_2$. The samples were incubated for 1 hour at 37 °C or overnight at 4 °C to confirm the efficacy of benzonase under these conditions. After incubation, GelRed (GelRed® Nucleic Acid Strain, Millipore, cat. No. SCT123) was added to each lysate, and RNA samples were prepared for separation using agarose gel electrophoresis. Volumes of individual components in the reaction mixtures with and without benzonase are recorded in Tab. VIII.

Table VIII: Reactions preparation with (2nd column) and without (3rd column) benzonase.

Reagent	Volume [μl]	Volume [μl]
Total RNA	2	2
CEB/MEB/NEB	10.5	13
MgCl$_2$ (20 mM)	1	0
Benzonase (10×)	1.5	0

4.8.1 Agarose gel electrophoresis

Agarose gel electrophoresis is a widely used method for the separation of nucleic acids according to their size. For our purposes, this method was mainly used to visualize the DNA/RNA status and confirm the effectiveness of benzonase under different conditions. 1.2 % agarose (Roti®Garose for DNA/RNA electrophoresis, Carl Roth, cat. No. 3810.4) gels in 1× TAE buffer (1 l, 50× TAE buffer, pH 8.3: 242 g TRIS-base; 18.6 g EDTA; 57.1 ml acetic-acid) were used. All samples were mixed with GelRed and heated for 5 minutes at 60 °C. Electrophoretic separation was run for approximately 1 hour at 100 V. The GelRed signal was subsequently viewed using bioimaging Syngene^{TM} Gbox Chemi XX6.

4.9 Immunoprecipitation using TBEV C-specific antibodies

The (co-)immunoprecipitation method was used for TBEV C and its interaction partners pull-down using Dynabeads[TM] Protein A magnetic beads (Invitrogen, Thermo Fisher Scientific, cat. No. 10002D) due to a high binding strength of protein A to guinea pig IgGs. The Dynabeads were vortexed before being washed twice in coIP buffer (50 mM TRIS, pH 7.4; 150 mM NaCl; 1 mM EDTA; 1 % NP-40). After the washing step, a primary antibody (anti-TBEV C; prepared in the Laboratory of Applied Biochemistry, FSc USB) was added in a ratio of 1:200. The anti-TBEV C antibody was incubated with the Dynabeads for 30 minutes at room temperature. The principle of this pull-down is shown in Fig. 8.
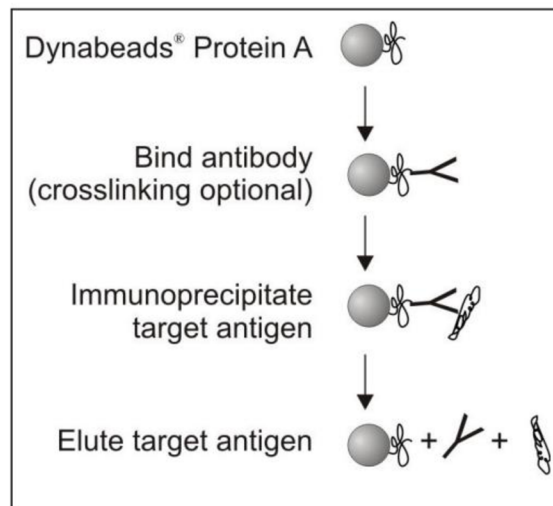
Figure 8: Principle of immunoprecipitation of antigen using Dynabeads[TM] Protein A (Product contents Dynabeads ® Protein A contains 30 mg Dynabeads ® /mL in phosphate, n.d.).

After incubation with the primary antibody, the supernatant was removed and 3 % BSA in coIP buffer was added in the same volume as in the step before. Blocking with BSA was done for 30 minutes at room temperature. Following that, the beads were washed twice in coIP buffer, and 50 µl of Dynabeads slurry with bound antibody was added to the previously prepared tubes with cytoplasmic, membrane, and nuclear extracts. Benzonase (10× Benzonase® Nuclease, ≥250 units/µl, Merck, cat. No. E1014) and 2 mM $MgCl_2$ were added to one set of samples. The incubation lasted overnight at 4 °C. The amount of protein lysates was calculated according to the BCA assay (Chapt. 4.5) and each sample contained approximately 22 µg of proteins. CoIP buffer with protease inhibitors (Halt[TM] Protease Inhibitor Cocktail) was added up to 250 µl.

The following day, the fraction containing unbound proteins (flow-through, F-T) was collected, which was stored until further use at -20 °C. The beads were washed four times in coIP buffer, and finally, 50 µl of NH₄HCO₃ (ammonium bicarbonate) was added to individual tubes. Bound proteins present in the elution fraction were subsequently identified using a timsTOF Pro mass spectrometer.

4.10 Protein identification by mass spectrometry (MS)

Protein identification by mass spectrometry was performed with the help of Mgr. Filip Dyčka, Ph.D. from the Laboratory of Proteomics, Department of Chemistry, FSc USB.

4.10.1 Trypsin digestion of proteins on magnetic beads

Bound proteins present in the elution fraction were identified using a timsTOF Pro mass spectrometer (Bruker Daltonics). Firstly, proteins were reduced by an addition of 50 µl of 10 mM DTT in 100 mM NH₄HCO₃ to the magnetic beads for 45 minutes at 56 °C. The next step was alkylation by an addition of 5 µl of 550 mM iodoacetamide in 100 mM NH₄HCO₃. The incubation took 20 minutes, and it was performed in the dark. Following that, 2,5 µl of 1M DTT in 100 mM NH₄HCO₃ was added to finish the alkylation process, and the incubation with DTT lasted for 15 minutes. Then, 50 µl of 100 mM NH₄HCO₃ were added followed by 0.2 µg of trypsin and the mixture was left to cleave overnight at 37 °C. The next day, the solution with peptides was acidified by adding 10 µl of 50 % formic acid (FA), and the peptides were purified using C18 StageTips according to a protocol by Rappsilber et al. (2007).

4.10.2 Protein identification using nanoLC-ESI MS/MS

The peptides were dissolved in 40 µl of 3 % acetonitrile/0.1 % formic acid, and their subsequent analysis was performed with the nanoLC Ultimate 3000 RSLSnano system (Thermo Fisher Scientific) on-line connected to a timsTOF Pro mass spectrometer. Parameters for the nanoLC separation and the mass spectrometer were the same as in Forinová et al. (2021). The data obtained by MS analysis was then processed in the program MaxQuant (versions 1.6.14.0 and 2.2.0.0) with the integrated browser Andromeda (Cox & Mann, 2008).

For protein identification, the human proteome database downloaded from Uniprot (8. 6. 2022) and databases of TBEV protein sequences and contaminant sequences implemented in the MaxQuant program were used. When searching in the MaxQuant program, the TIMS-DDA and Bruker TIMS instrument parameters were left in the basic settings. Other used parameters were: Trypsin/P enzyme in specific digestion mode

with the possibility of up to two missed cleavage sites, carbamidomethylation of cysteine as a fixed modification, oxidation of methionine as a possible modification, minimum peptide length of 5 amino acids, precursor tolerance of 20 ppm in the first and 10 ppm in the second peptide search, tolerance for MS/MS fragments of 25 ppm.

Assigned spectra (peptide spectrum match, PSM) and identified proteins were further filtered using a target-decoy approach with a 1 % false discovery rate (FDR) setting. The algorithm integrated in the MaxQuant program was used to perform label-free quantification (LFQ) and intensity-based absolute quantification (iBAQ). The data obtained from MaxQuant were further processed in the Perseus program (version 2.0.9.0; Tyanova & Cox, 2018). Contaminants, proteins from the reverse database, and proteins identified only based on modified peptides were excluded. Protein quantification intensities (LFQ or iBAQ) were logarithmically transformed to base 2. Proteins that were identified by only 1 peptide and whose scores did not reach 40 were excluded from further analysis.

5 Results

5.1 Optimization of nuclear and cytoplasmic fraction isolation

The first part of this thesis was focused primarily on the optimization of nuclear and cytoplasmic fraction isolation since plenty of different techniques and approaches have existed, including commercially available kits as well as home-made methods. For these reasons, we decided to test three methods: (1) NE-PER extraction and subcellular protein fractionation using the NE-PER^{TM} Nuclear and Cytoplasmic Extraction Reagents Kit (Thermo Fisher Scientific); (2) subcellular protein fractionation using the Subcellular Protein Fractionation Kit for Cultured Cells (Thermo Fisher Scientific); and (3) rapid isolation of nuclei cells *in vitro* performed according to the protocol by Nabbi & Riabowol (2015), including the preparation of fresh home-made buffers and several centrifugation steps.

For all experiments, we used the human medulloblastoma cell line DAOY. Cells were first seeded in a 6-well plate (0.5×10^6 cells per well) and infected 1 day post seeding by TBEV-Eu isolate Hypr (5 MOI). At 24 hours post infection, cells were harvested following the instructions of the respective method of fractionation. The graphic scheme of the whole process in subsequent steps is recorded in Fig. 9.
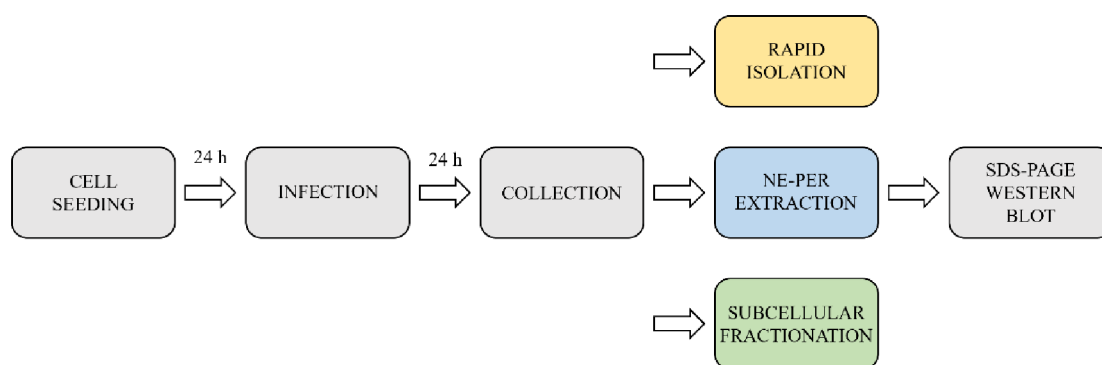
Figure 9: Optimization of individual fraction isolation methods in subsequent steps including cell seeding, infection, collection, rapid isolation, NE-PER extraction, subcellular fractionation, SDS-PAGE, and WB.

Verification of each fraction purity was then done by SDS-PAGE (12 % gels) and WB detection of markers specific for cytoplasmic (beta III-tubulin; TUBB3), cytoskeletal (vimentin; VIM), and nuclear (lysine Specific Histone Demethylase 1; KDM1/LSD1) fraction. All experiments were performed in two biological replicates for each marker, and each lysate applied to the gel contained the same amount of proteins (4 000 ng).
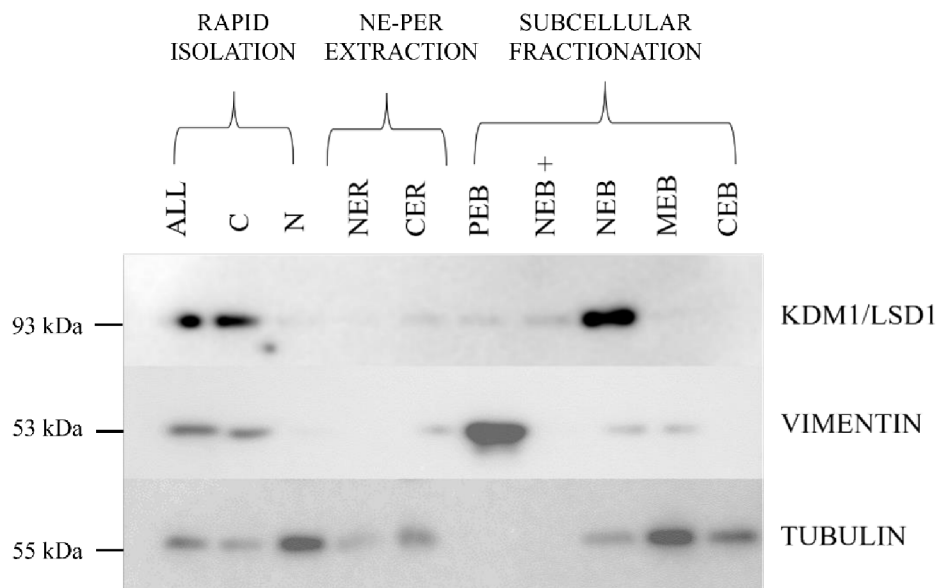
Figure 10: Optimization of individual fraction isolation. The first row shows the detection of the nuclear marker KDM1/LSD1, the second row the detection of the cytoskeletal marker vimentin, and the third row the detection of the cytoplasmic marker tubulin. The first three samples were prepared by the rapid isolation method. ALL indicates whole cell lysate, C cytoplasmic fraction, and N nuclear fraction. The next set of samples was isolated by NE-PER extraction method, where NER stands for the nuclear extract and CER for the cytoplasmic extract. The last five samples were prepared by subcellular protein fractionation method. PEB indicates the cytoskeletal fraction, NEB+ the chromatin-bound fraction, NEB the nuclear fraction, MEB the membrane fraction, and CEB the cytoplasmic fraction.

Fig. 10 illustrates that the cytoplasmic and nuclear fractions were best separated by the subcellular fractionation method, when the detection of individual markers shows strict separation (especially for the nuclear marker KDM1/LSD1). There was a problem with samples prepared by NE-PER extraction due to the weak detection in both cytoplasmic and nuclear fractions. In the case of the rapid nuclear isolation method, fractions were probably not fully separated, as the signal for KDM1/LSD1 (a nuclear marker) was present in the cytoplasmic fraction together with vimentin. According to these results, the Subcellular Protein Fractionation Kit for Cultured Cells was selected for further experiments.

5.2 Benzonase digestion optimization and the effect of $MgCl_2$ on its efficacy

After the optimization of cellular fraction isolation, we prepared four sets of samples to optimize Benzonase[®] Nuclease (benzonase) cleavage. This non-specific DNase and RNase was used to ensure the degradation of all DNA and RNA in samples, thereby eliminating the identification of false-positive nucleic acid-mediated binding partners. Each set comprised CEB, MEB, or NEB lysates mixed with 2 µg of total RNA isolated from DAOY cells. Sets 1 and 2 were incubated with or without benzonase. Analogically, sets 3 and 4 were incubated with or without benzonase as well, however, with the addition of $MgCl_2$ in a final concentration of 2 mM. Agarose gel electrophoresis was used to visualize the RNA integrity status and confirm the effectiveness of benzonase digestion under different conditions.
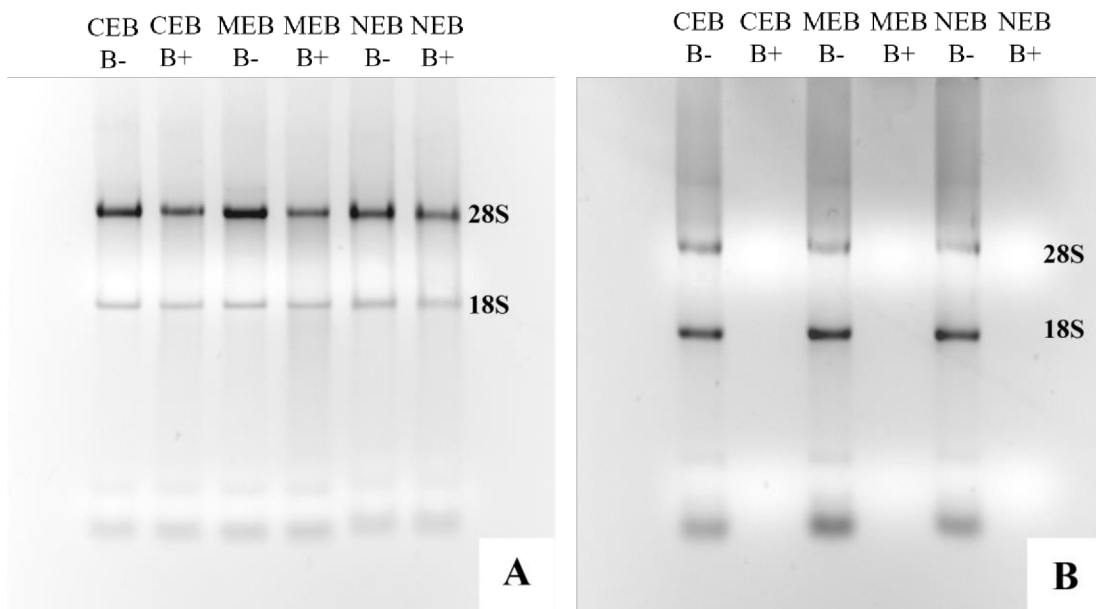
Figure 11: Benzonase treatment optimization. 28S refers to 28S ribosomal RNA, and 18S refers to 18S ribosomal RNA. CEB indicates the cytoplasmic fraction, MEB the membrane fraction, and NEB the nuclear fraction. B- indicates samples without benzonase, and B+ samples with benzonase. A shows the gel electrophoresis with the B+ samples without 2 mM $MgCl_2$ incubated for 1 hour at 37 °C. B shows the gel electrophoresis with the B+ samples with $MgCl_2$ incubated overnight at 4 °C.

Based on the results in Fig. 11, we confirmed that the addition of $MgCl_2$ to the samples is required for complete RNA degradation. Samples incubated overnight at 4 °C (Fig. 11B) confirmed the efficacy of benzonase under these conditions.

5.3 Immunoprecipitation optimization using TBEV C-specific antibodies

Simultaneously with the benzonase digestion optimization, the immunoprecipitation specificity of TBEV C using TBEV C-specific antibodies and various cell fraction lysates was optimized. For all experiments, we used the human medulloblastoma cell line DAOY. These cells were first seeded in a 25 cm^2 flask (2×10^6 cells/flask), and the next day, they were infected by TBEV-Eu isolate Hypr (5 MOI). After 24 hours, I harvested the cells and performed the subcellular fractionation. The immunoprecipitation itself consisted of several steps (Fig. 12). The washed beads (Dynabeads^{TM} Protein A) were first incubated with the primary antibody (anti-TBEV C) for 30 minutes and then blocked in 3 % BSA in coIP buffer for the same time. Finally, each lysate (CEB, MEB, or NEB) with benzonase was added to the appropriate tube, and the beads were incubated overnight at 4 °C. The second day, the F-T and elution fractions were collected, and SDS-PAGE electrophoresis with WB detection was used to confirm the presence of TBEV C in individual fractions to prove the specificity of TBEV C immunoprecipitation with the beads.

Figure 12: Immunoprecipitation procedure in consecutive steps including Dynabeads incubation with the primary antibody (ant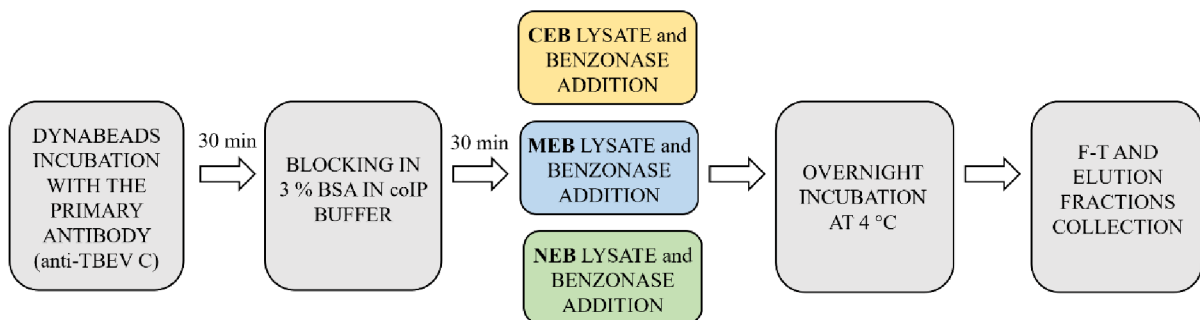i-TBEV C), blocking in 3 % BSA in coIP buffer, individual lysate and benzonase addition, overnight incubation at 4 °C, and F-T and elution fractions collection.
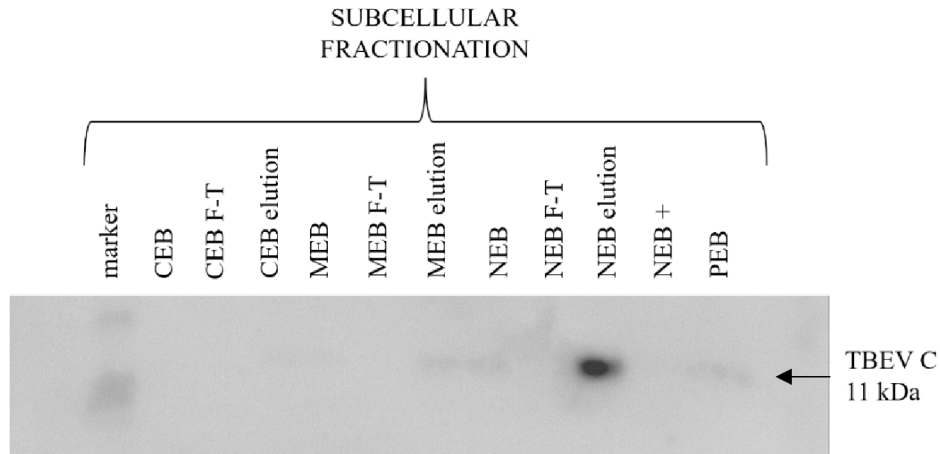
Figure 13: Optimization of immunoprecipitation using TBEV C-specific antibodies. CEB (cytoplasmic fraction), MEB (membrane fraction), and NEB (nuclear fraction) represent input samples subjected to immunoprecipitation. Samples labelled "elution" indicate samples released from magnetic beads, and samples labelled "F-T" indicate flow-through fractions. NEB + is the chromatin bound fraction, and PEB is the cytoskeletal fraction. As a size standard, Protein Marker VI (10-245) prestained (AppliChem, cat. No. A8889) was used.

As can be seen in Fig. 13, TBEV C (11 kDa) was detected mainly in the nuclear fraction (NEB elution and NEB). Weak detection was described also in the membrane fraction (MEB elution and MEB); however, no TBEV C signal was detected in the cytoplasmic fraction. Additionally, the cytoskeletal fraction (PEB) showed a weak presence of TBEV C as well. With these findings, we verified the functionality of the protocol and confirmed the specificity of TBEV C binding to the magnetic beads via specific antibodies. Same procedure was then used for co-immunoprecipitation of TBEV C interacting partners.

5.4 TBEV C detection and subcellular distribution

During the preparation of co-immunoprecipitation samples for MS identification, TBEV C detection by the WB was found to be challenging. For that reason, a set of experiments was performed with different SF lysates and various amounts of input proteins in individual samples to optimize TBEV C detection. Furthermore, as an alternative to DAOY cells, we used the A549 cell line. Cells were first seeded in a 25 cm^2 flask (2×10^6 cells/flask) and then infected by TBEV-Eu isolate Hypr (5 MOI) the next day. After 24 hours, any signal was not observed for TBEV C; therefore, the infection period was extended by 12 hours (i.e., 36 hpi). Then, the cells were collected, and individual fractions

were isolated using the Subcellular Protein Fractionation Kit for Cultured Cells. SDS-PAGE was performed on 15 % gels and WB was done using the anti-TBEV C antibodies.
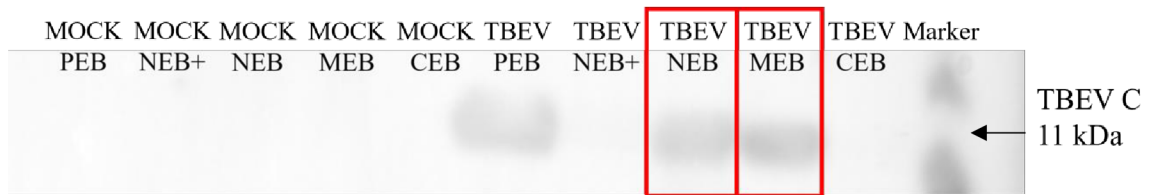
Figure 14: TBEV C detection in individual fractions of A549 cells. The samples were prepared by the subcellular protein fractionation method, and the amount of protein applied to the gel was 4 000 ng. TBEV stands for the samples infected by TBEV-Eu isolate Hypr (5 MOI), and MOCK for samples infected by brain suspension from uninfected mice. PEB indicates the cytoskeletal fraction, NEB+ the chromatin-bound fraction, NEB the nuclear fraction, MEB the membrane fraction, and CEB the cytoplasmic fraction. As a size standard, Protein Marker VI (10-245) prestained (AppliChem, cat. No. A8889) was used.

The results depicted in Fig. 14 show the TBEV C detection and its subcellular distribution, mainly in the membrane, nuclear, and cytoskeletal fractions, which was consistent with our previous observations (see Fig. 13). To finalize the protocol for obtaining the samples with detectable amount of TBEV C, we decided to repeat the previous experiment, this time with nuclear extracts only. Both DAOY and A549 cells were used with different input total protein amounts in each sample.
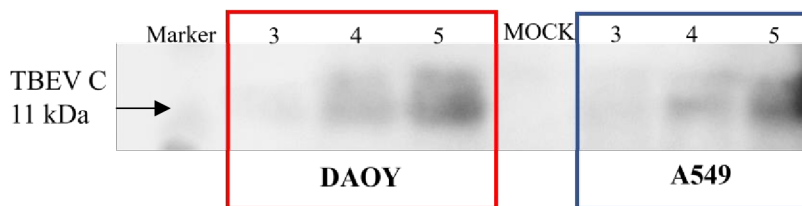
Figure 15: TBEV C detection in different input amounts of protein lysates from TBEV infected cells. The DAOY (red) and the A549 (blue) cells were infected by the TBEV-Eu isolate Hypr (5 MOI). MOCK indicates a cell sample treated with brain suspension from uninfected mice. After 36 hpi, all NEB (nuclear) extracts were prepared by the subcellular fractionation method, and the amount of protein applied to the gel was 3 000 ng, 4 000 ng and 5 000 ng for each cell line lysate. As a size standard, Protein Marker VI (10-245) prestained (AppliChem, cat. No. A8889) was used.

TBEV C is detected in both A549 and DAOY cells in all tested concentrations (3 000 ng, 4 000 ng, and 5 000 ng; Fig. 15), thus it was decided in further experiments to collect cells and perform SF at 36 hpi and use 4 000 ng of protein lysates.

5.5 MS identification of TBEV C and its binding partners

In the Tab. IX an overview of all MS identification attempts is summarized. It provides all pertinent information, including assigned measurement number (1–5), the experiment type, sample collection after incubation with the virus, benzonase treatment, blocking in 3 % BSA in the coIP buffer, and the type of identified fractions.

Table IX: MS identification overview.

	Experiment	*Collection*	*Benzonase*	*Blocking*	*Fractions*
1	MS optimization	24 hpi	+	no	CEB/MEB/NEB
2				yes	only NEB

3	MS identification (1)	36 hpi	+/-	yes	CEB/MEB/NEB
4	MS identification (2)				
5	MS identification (3)				

5.5.1 MS optimization progress

After adjusting all previous steps, optimization of the MS identification of TBEV C and its binding partners was also performed. DAOY cells were seeded in a 25 cm^2 flask (2×10^6 cells/flask) 1 day prior to the infection with the TBEV-Eu isolate Hypr (5 MOI). Sampling took place 24 hours after the infection, and immediately following that, individual fractions (CEB, MEB, and NEB) were separated. Co-immunoprecipitation of TBEV C and its binding partners (including benzonase digestion) was performed afterwards, and the samples containing the elution fraction were handed over to Mgr. Filip Dyčka, Ph.D. for the ensuing identification using mass spectrometry.

The presence of many interacting human proteins was demonstrated by the initial MS results. Surprisingly, more proteins were identified in the control (MOCK) samples, lacking any TBEV C protein when compared to the infected samples. The reason could have been sample swapping. To exclude this option, other viral proteins (TBEV NS3 and TBEV NS5) were searched for in these eluted fractions. However, MS disproved this theory, as viral proteins NS3 and NS5 were identified in samples annotated as infected (Fig. 16). To increase the specificity, in the following repeated experiment, an addition of 3 % BSA for blocking non-specific bindings was used.
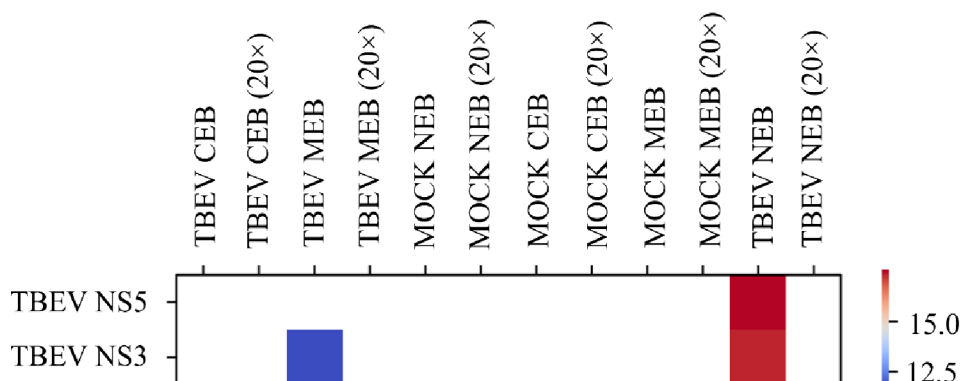
Figure 16: Identification of viral proteins NS5 and NS3 in the initial MS optimization (1). TBEV indicates infected samples, and MOCK indicates non-infected samples. CEB stands for the cytoplasmic fraction, MEB for the membrane fraction, and NEB for the nuclear fraction. The first row shows the NS5 detection, and the second row shows the NS3 detection. LFQ stands for label-free quantification, and 20× represents samples that have been diluted 20 times. The colour scale shows the intensity-based absolute quantification (iBAQ). All values are plotted in the log2.

In the second MS optimization experiment (2), only nuclear (NEB) fractions from three different biological replicates were used for a better overview during evaluation. Additional essential data on the preparation of these fractions by co-immunoprecipitation are included in Tab. IX. Inclusion of the blocking step has shown to be functional as the amount of non-specific binding protein interactions was reduced. Overall, however, only a small number of proteins was identified, including many apolipoprotein variants and immunoglobulin chains (Tab. X).

Table X: Top 5 proteins identified in the second MS optimization attempt (2).

	Protein name	*Gene*	*UniProt ID*
1	Apolipoprotein A-I, isoform CRA_a	APOA1	A0A024R3E3
2	Alpha-2-HS-glycoprotein	AHSG	C9JV77
3	Apolipoprotein A-II	APOA2	V9GYE3
4	Haptoglobin	HP	P00738
5	IGL@ protein	IGL@	Q6GMW3

The small number of identified interaction partners combined with the documented non-specific binding of TBEV C to RNA/DNA (Kaufman et al., 2020) led me to a new hypothesis: TBEV C directly interacts with other proteins only sporadically, and most of the binding potential is mediated by RNA/DNA molecules. Identified binding proteins in studies that do not account for these interactions are then a false positive signal due to the TBEV C co-immunoprecipitation and a non-interacting protein that are bound to the same RNA/DNA molecule. Therefore, for further experiments, the presence and absence of benzonase treatment during sample preparation was included to verify whether this reasoning is correct. Also, cell sampling and performing SF was performed after 36 hpi due to the results described previously in Chap. 5.4.

5.5.2 MS identification of individual TBEV C interactomes

Three biological replicates of co-immunoprecipitation and MS identification of TBEV C interacting proteins were performed (see Tabs. XIV, XV, and XVI in the supplementary data). All samples were prepared according to the protocol specified in Chapt. 4.9. Individual samples of each fraction (CEB, MEB, and NEB) were split into two, and TBEV C-interacting DNA/RNA was digested with benzonase in one of them. Co-immunoprecipitation reactions were incubated overnight at 4 °C, including individual extracts (22 µg of proteins) and the primary antibody in a ratio of 1:200 (anti-TBEV C). After co-immunoprecipitation, the eluted fractions were used for MS identification.

From the lists of identified proteins, contaminants were first removed. A summary tables for all three biological replicates and for the infected samples only were generated that contained the identified proteins with the highest scores for each interactome (i.e., CEB, MEB, and NEB). Unfortunately, only a few of the identified proteins were found simultaneously in at least two biological replicates (mostly in fractions without benzonase). Also, no significant differences in the number of identified proteins between samples with and without benzonase treatment were revealed, except for the MEB fraction, in which after benzonase treatment, the number of identified proteins rapidly decreased. Therefore, for further analysis, only samples containing benzonase were used, and the top-ranked and most interesting interacting proteins of the cytoplasmic TBEV C interactome (Tab. XI), membrane TBEV C interactome (Tab. XII), and nuclear TBEV C interactome (Tab. XIII) are described in the corresponding tables. All heatmaps for each measurement are included in the supplementary data (see Tabs. XIV, XV, and XVI).

Table XI: Cytoplasmic TBEV C interactome.[1]

	Protein name	Gene	UniProt ID	log2_iBAQ MS (1)		log2_iBAQ MS (2)		log2_iBAQ MS (3)		Function
				B+	B-	B+	B-	B+	B-	
1	Transmembrane emp24 domain – containing protein 2	TMED2	F5GX39	×	×	×	×	15.7	11.5	protein transport
2	Synaptophysin-like protein 1	SYPL1	H7C4J8	×	×	×	×	14.8	×	synaptic transmission
3	Cleft lip and palate transmembrane protein 1	CLPTM1	K7EJ16	×	×	×	×	14.7	×	protein transport
4	Transmembrane emp24 domain-containing protein 9	TMED9	B2R8A2	×	×	×	×	14.6	×	protein transport
5	Large neutral amino acids transporter small subunit 1	SLC7A5	Q96QB2	×	×	×	×	14.3	13.1	amino acid transport
6	Peroxisomal membrane protein 4	PXMP4	B4DLI8	×	×	×	×	14.2	×	protein transport
7	Thymosin beta-10	TMSB10	P63313	14.1	×	×	×	×	×	cytoskeleton organization
8	Transmembrane protein 97	TMEM97	Q86XC5	×	×	×	×	13	×	protein transport
9	Multidrug resistance-associated protein 1	ABCC1	G0ZCM3	×	×	12.9	×	×	×	ATP-binding
10	Gamma-secretase subunit PEN2	PSENEN	Q9NZ42	×	×	×	×	12.9	×	cleavage catalysation
+	TBEV NS5	-	-	×	×	×	×	8	8.6	genome replication
+	Glyceraldehyde-3-phosphate dehydrogenase (GAPDH)	HEL-S-162eP	V9HVZ4	×	11.1	×	×	×	×	glycolysis, oxidoreductase

[1] × indicates no available measured data (no detection in the individual fraction section) and – indicates no available UniProt data (same for the Tabs. XI, XII, XIII)

36

Table XII: Membrane TBEV C interactome.

	Protein name	Gene	UniProt ID	log2_iBAQ MS (1)		log2_iBAQ MS (2)		log2_iBAQ MS (3)		Function
				B+	B-	B+	B-	B+	B-	
1	Clathrin light chain B	CLTB	A0A024R7S3	13.4	13.6	×	9.8	×	×	protein transport
2	Histone H2B type 1-H	HIST1H2BH	Q93079	12.2	×	×	×	×	×	nucleosome component
3	TBEV NS3	-	-	11	11.3	×	×	×	×	serine-protease activity
4	Spectrin alpha chain (non-erythrocytic 1)	SPTAN1	A0A0D9SFF6	10.1	11.7	×	×	×	×	secretion
5	Large neutral amino acids transporter small subunit 1	SLC7A5	Q96QB2	×	×	×	×	9.2	12.6	amino acid transport
6	TBEV NS5	-	-	×	×	×	×	8.7	×	genome replication
+	60S ribosomal protein L23a	K7EMA7	RPL23A	×	×	×	11.6	×	×	ribosomal protein, translation
+	Alpha-enolase	A0A2R8Y798	ENO1	×	×	×	15.4	×	×	glycolytic process

Table XIII: Nuclear TBEV C interactome.

	Protein name	Gene	UniProt ID	log2_iBAQ MS (1)		log2_iBAQ MS (2)		log2_iBAQ MS (3)		Function
				B+	B-	B+	B-	B+	B-	
1	Transketolase	TKT	F8W888	15.8	×	×	×	×	×	glycolysis, transferase
2	Epididymis luminal protein 2	HEL2	V9HW98	15.1	×	×	×	×	×	regulation protein
3	Histone H2A	MACROH2A1	D6RCF2	14.7	×	×	×	×	×	nucleosome component
4	Glyceraldehyde-3-phosphate dehydrogenase (GAPDH)	HEL-S-162eP	V9HVZ4	14.4	11.4	×	×	×	×	glycolysis, oxidoreductase
5	Lactate dehydrogenase A	LDHA	F5GXY2	14.2	10.1	×	×	×	×	glycolysis, oxidoreductase
6	Heterogeneous nuclear ribonucleoprotein L	HNRNPL	M0QYL7	14	12.6	×	×	×	×	RNA-binding
7	Calreticulin	CALR	B4E2Y9	14	×	×	×	×	×	protein folding
8	Transmembrane emp24 domain-containing protein 2	TMED2	F5GX39	13.5	×	×	×	×	×	protein transport
9	Heterogeneous nuclear ribonucleoprotein A1	HNRNPA1	A0A7I2YQY2	×	×	13.3	×	×	×	RNA-binding
10	Transmembrane emp24 domain-containing protein 7	TMED7	Q3B7W7	13.2	×	×	×	×	×	protein transport
+	TBEV NS5	-	-	×	×	×	×	8	8.7	genome replication
+	Histone H2B type 1-H	HIST1H2BH	Q93079	12.6	10.7	×	×	×	11.9	nucleosome component
+	Alpha-enolase	A0A2R8Y798	ENO1	×	×	×	15.2	×	×	glycolytic process

In summary, from the extensive results review (Tabs. XI, XII, and XIII), the following was observed:

- Although each sample submitted for MS identification contained the same input number of proteins (22 μg), this amount might still be insufficient to capture and identify less abundant proteins. This can be the cause of the high variation between the proteins retrieved in individual replicates and inability to capture TBEV C in any sample.

- There was no significant difference in protein identification between samples with and without benzonase treatment, except for the MEB fraction, in which after benzonase treatment, the number of identified proteins rapidly decreased.

- Only a small number of proteins (mostly in fractions without benzonase) were identified jointly in at least two biological replicates with significant scores; however, some proteins were identified with lower scores in all fractions (for example: TBEV NS5 which was detected with a lower score also in the CEB and NEB fraction, thus confirming the NS5 nuclear localization).

- Some interacting proteins were identified jointly in two fractions. For cytoplasm and membranes (the CEB and MEB fractions) that was, for example, SLC7A5, and for cytoplasm and nucleus (CEB and NEB fractions) TMED2.

- Many glycolytic enzymes (for example: TKT, GAPDH, and LDHA) were found to interact with TBEV C mainly in the nucleus.

- The most universal interacting partner detected, commonly for the nucleus and membranes (the NEB and MEB fraction) was the histone protein HIST1H2BH.

6 Discussion

The family *Flaviviridae* consists of 4 genera, of which the most important is the genus *Flavivirus*, which includes globally known arboviruses such as DENV, ZIKV, or WNV (Simmonds et al., 2017). These viruses circulate worldwide, and their geographic distribution is increasing since the human population is growing along with increasing tourism and climate changes caused by global warming (Barrows et al., 2018). Every year, several hundred million people suffer from infections caused by flaviviruses. Tens of thousands of infected subsequently succumb to the infection and thousands more develop long-term disabilities, making these viruses one of the main public health concerns (Mazeaud et al., 2018).

TBEV, a tick-borne member of *Flavivirus* genus, accounts for one of the highest incidence rates of flaviviral infections in Eurasia, where more than 13 000 cases of TBEV infection are reported annually (Lindqvist et al., 2018). Importantly, under the impact of climate changes, TBEV is spreading further to the western and northern regions of Europe and to higher altitudes (Orlíková et al., 2021). Since there is no specific therapy for TBEV available (Kaufman et al., 2020) and TBEV infection often leads to life-long neurological complications (Pulkkinen et al., 2018), there are more and more efforts to find a target for drug development, of which the capsid protein (C) is a promising candidate (Sotcheff & Routh, 2020).

The formation of nucleocapsids is the most significant role of TBEV C. Its ability to bind the viral RNA and function in promoting the proper assembly of infectious particles makes it a crucial regulatory viral protein in infected cells (Kemenesi & Bányai, 2019). Even more attention has been paid to this protein since its nuclear localization was documented. Almost all TBEV C functions take place in the cytoplasm or endoplasmic reticulum, and to this day, only few details are known about the role of TBEV C in the nucleus (Selinger et al., 2022). For these reasons and getting closer to finding out more about TBEV C function in the nucleus, the primary aim of this work was to identify the TBEV C interaction partners in the nuclear and cytoplasmic fraction of infected cells.

Before starting the work, it was first necessary to optimize all methods and conditions, since no study has yet been created that would study the interactome of given subcellular fractions in a similar way. During the work, it was also faced many challenges with the method of subcellular fractionation, (co-)immunoprecipitation, and the detection of TBEV C itself. This study, therefore, presents an initial work in progress, which requires further research to present substantiated evidence.

Firstly, the subcellular fractionation method had to be optimized. The commercially available Thermo Fisher Scientific Subcellular Protein Fractionation Kit for Cultured Cells was selected to be used for all experiments due to the strict separation of nuclear and cytoplasmic fractions in contrast with other methods (rapid isolation of nuclei cells *in vitro* and NE-PER nuclear and cytoplasmic extraction) and the stable results that were obtained from the detection of the fraction-specific markers (TUBB3, VIM, and KDM1/LSD1). Also, the extensive advantage of using this commercial kit was the previous optimization as part of my bachelor thesis (Jaklová, 2021). However, as it turned out, many proteins that were localized in a different fraction than would be expected were identified. Also, the abundance of some proteins calculated based on the iBAQ data was the same for the CEB and MEB fractions (for example: SLC7A5) or for the CEB and NEB fractions (for example: TMED2). According to the product overview, each subcellular compartment may exhibit 15 % contamination between fractions, which is sufficient purity for almost all experiments studying protein localization and redistribution. However, protein identification by MS is quite sensitive, and 15 % contamination between fractions is too high, thus, a different method with as low contamination as possible was needed. For this reason, the separation of fractions by ultracentrifugation will be used in the future as an alternative (see Geladaki et al., 2019).

After optimizing SF, (co-)immunoprecipitation and the use of benzonase to eliminate false-positive nucleic acid-mediated interaction partners was optimized. Although each sample submitted for co-immunoprecipitation contained the same number of proteins (approximately 22 µg), this apparently results in a small amount of purified interacting proteins due to the fact that even TBEV C was not detected in any of these samples. A main concern with MS analysis is the incomplete sampling of peptide ions. Often, it is the more abundant proteins that are detected more readily, and this has often resulted in the loss of peptide identification belonging to the less abundant proteins, making comparisons within and between subcellular proteomes challenging (Lee et al., 2010). So, it might be wise to provide more proteins for MS identification in the future (exactly how much needs to be verified).

Also, only a small number of proteins were identified in at least 2 biological replicates (mostly in fractions without benzonase). When preparing further experiments, it would therefore be more advantageous not to have such long gaps between measurements but to always give three sets from each fraction at the same time for the MS identification. However, some proteins were identified with different scores in all fractions,

for example: TBEV NS5, which was detected with a lower score also in the CEB and NEB fraction, thus confirming the NS5 nuclear localization shown, for example by Jaklová (2021).

Based on these results, it is also clear that there was no significant difference between samples with and without benzonase, except for the MEB fraction, where overall fewer proteins were identified and, after benzonase treatment, the number of identified proteins rapidly decreased. This is what would be expected to be seen for all three fractions since the number of interacting proteins should be reduced to only protein-protein interactions, not mediated by nucleic acids.

6.1 TBEV C targets histones (H2A and H2B) during TBEV infection

The most surprising finding was the identification of HIST1H2BH (histone H2B) as a TBEV C interacting partner in the MEB fraction. Histone proteins are the major chromatin components that affect many biological processes, including gene regulation and transcription, replication, mitosis, and apoptosis (Shechter et al., 2007). Since they are part of the nucleosome, it would be expected that they would be present in the nuclear fraction.

The HIST1H2BH MEB localization was probably not caused due to the contamination by the incomplete removal of the previous extract during the subcellular fractionation process since first the membrane and then the nuclear fraction were isolated. The most likely cause could be the early on nuclear separation within the membrane fraction. However, according to the article presented by Colpitts et al. (2011) dealing with DENV C and the identification of the potential binding partners of this protein in the human liver cells, DENV C targets the four core histones H2A, H2B, H3, and H4. C protein might bind the newly formed histones and thus retain them in the cytoplasm.

It has been demonstrated that DENV C binds recombinant histones in solution and colocalizes with them in the nucleus and cytoplasm during the DENV infection (Fig. 17; Colpitts et al., 2011). According to this article and considering all findings, it is highly possible that flaviviral C protein acts as a histone mimic, forming heterodimers with core histones, binding DNA, and disrupting nucleosome formation (Colpitts et al., 2011). Since the C protein has many common features and functions across all flaviviruses, we might expect a similar function in TBEV C as well.
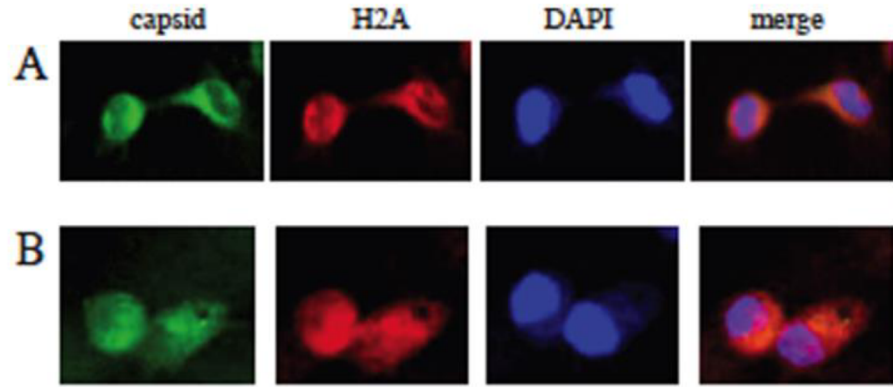
Figure 17: DENV C co-localization with histones during the DENV infection. Huh7 cells were infected with the human South American isolates of dengue 1 and fixed 24 hpi with 4 % paraformaldehyde. Cells were stained with antibodies against histone H2A and counterstained with DAPI to visualize the nucleus. DENV C is green, histone staining is red, and 4′,6-diamidino-2-phenylindole (DAPI) is blue (Colpitts et al., 2011).

In the case of MEB localization, further investigation would be necessary; however, based on the results presented by Liao et al. (2021) dealing with the histone (H2B) as an alternative cellular receptor for *Mycoplasma genitalium* protein of adhesion (MgPA), MEB localization was documented using both fluorescent microscopy (Fig. 18) and WB (Fig. 19).
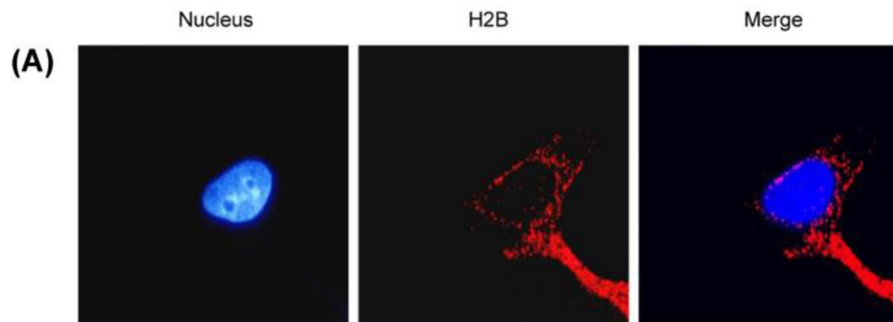

Figure 18: Subcellular localization of histone H2B protein in SV-HUC-1 cells (epithelial cells isolated from the uroepithelium). The red fluorescence representing H2B was observed on the cell membrane and in the cytoplasm and nuclear region. Nuclei were stained with DAPI (blue; Liao et al., 2021).
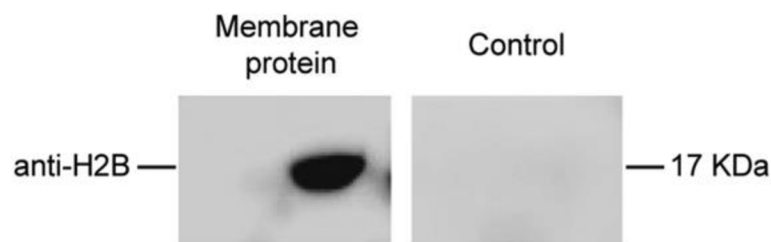
Figure 19: The anti-histone H2B antibody binding to a 17 kDa membrane protein. Isolated SV-HUC-1 membrane proteins were incubated with H2B antibody, resulting in a clear band at a molecular weight of about 17 kDa in the experimental group, while no band appeared in the control group which was not incubated with H2B antibody (Liao et al., 2021).

The overall identification of HIST1H2BH in membrane/nuclear, and MACROH2A1 (histone H2A) in the nuclear fraction as the important parts of the TBEV C interactome presented in this study could indicate the important role of this protein in the host cell during infection – with the possibility that C protein may target core histones to interfere with the host cell genetic machinery in order to promote the viral replication.

6.2 TBEV C interacts with the NEB-specific glycolytic enzymes

Another important finding was the identification of glycolytic proteins (in particular GAPDH, LDHA, and TKT) within the nuclear interactome of TBEV C. A biological process called glycolysis converts glucose into pyruvate to produce ATP (Jung et al., 2014). The characteristics of glycolytic enzymes structures and catalysis are well known; however, the link between glycolytic proteins and their involvement in viral infection is still unclear.

GAPDH has been previously observed in the nuclear fraction, for example in a bachelor thesis presented by Jaklová (2021), where GAPDH detection using WB was noted in all fractions (CEB, MEB, NEB, and NEB+) except PEB (cytoskeletal fraction; Jaklová, 2021). This can be explained by the fact that GAPDH, in addition to its role in glycolysis, also initiates the cascade of programmed cell death – apoptosis (Sen et al., 2008). It has been found that under stress conditions, apoptotic stimuli can activate iNOS (inducible NO synthase), which nitrosylates GAPDH and thereby activates its import into the nucleus (Sen et al., 2008). In the nucleus, GAPDH stimulates p300/CREB acetyltransferase activity, leading to the activation of the expression of the pro-apoptotic gene p53 (Sen et al., 2008). Since the process of infection is considered a stress factor, nuclear localization of GAPDH is more than possible.

44

The conversion of pyruvate to lactate is catalysed by the canonical enzyme activity of LDHA, which has been found to play a crucial role in cancer development (Liu et al., 2018) and was also identified as one of the nuclear interaction partners of TBEV C. It is widely known that LDHA localizes in the cytoplasm and produces lactate there. In addition, it was shown that nuclear LDHA detects reactive oxygen species (ROS) and gains a new catalytic function to support human papillomavirus (HPV)-induced cervical carcinogenesis (Liu et al., 2018). LDHA senses excessive ROS with a tetramer-to-dimer transition and nuclear translocation in response to HPV infection or oxidative stress (LDAH nuclear localization in Fig. 20).
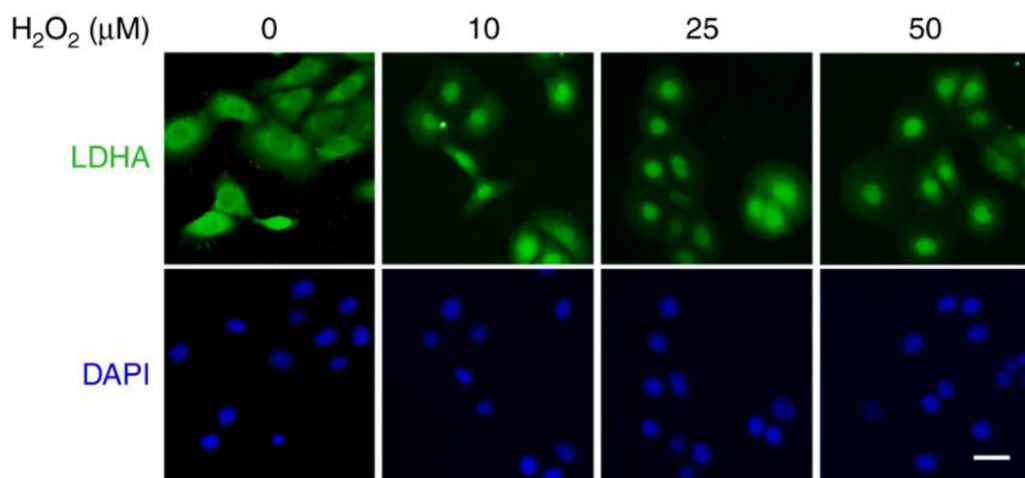
Figure 20: LDHA nuclear translocation profoundly increasing in an H_2O_2-dose-dependent manner. LDHA (green) in HaCaT cells upon different doses of H_2O_2 treatment as indicated. DAPI is blue, and the scale bar is 10 μm (Liu et al., 2018).

Nuclear LDHA develops a noncanonical enzymatic activity to generate the antioxidant metabolite, α-HB, which can shield cervical cancer cells from severe oxidative stress and stimulate cell growth via epigenetic regulations (Liu et al., 2018). It is interesting to note that cell proliferation and redox equilibrium seem to depend on LDHA nuclear translocation, and since the LDHA nuclear localization has been observed in multiple cancer types, including colorectal cancer, breast cancer, prostate cancer, lung cancer, or liver cancer (Liu et al., 2018), it is highly possible that LDHA may play an important role in the TBEV-infected medulloblastoma cells and interacts with the TBEV C in order to fight against infection through cell protection and cell growth stimulation.

Another protein identified within the TBEV C nuclear interactome was TKT. Cancer cells can modify their metabolism to adjust to changes in the microenvironment. The Warburg effect, which causes glycolysis and the pentose phosphate pathway (PPP) to rise even in the presence of oxygen, is the most well-known metabolic aberration in cancer cells. TKT, a crucial enzyme in the non-oxidative phase of PPP, catalyses a string of reversible processes connecting PPP to glycolysis and creating a dynamic network in the non-oxidative phase (Qin et al., 2019). This gives PPP the ability to change the metabolic pattern to satisfy the various needs of cancer cells under various stressful circumstances. In the study presented by Qin et al. (2019), TKT showed a strong nuclear localization, which might indicate the possibility that nuclear TKT might play a non-metabolic role to promote the development of HCC cells or other cancer cells (in our case the medulloblastoma cells).

Based on all of these discoveries, it is highly probable that GAPDH, LDHA, and TKT may interact with TBEV C, although the precise mechanism and function are yet unknown. Therefore, findings described in this thesis need be further experimentally verified.

6.3 Comparison with the TBEV C whole-cell interactome shows differences

In the work presented by Selinger et al. (2022), the whole-cell TBEV C interactome was described (Fig. 21). The obtained data revealed 213 interacting proteins, including viral proteins E and NS5. Surprisingly, the TBEV C interactome did not contain any of the DENV, WNV, or ZIKV C proteins previously known interaction partners (Selinger et al., 2022). These include SEC3p (negative regulator of flavivirus transcription and translation; Bhuvanakantham & Ng, 2013), APOE and PLIN3 (surface proteins of lipid droplets; Carvalho et al., 2011; Martins et al., 2019), UPF1 and PYM1 (factors functionally engaged in nonsense-mediated mRNA decay; Fontaine et al., 2018; Li et al., 2019). The only exception was the nucleolar protein NPM1/B23, which has been demonstrated to interact with the DENV (Balinsky et al., 2013) and JEV C (Tsuda et al., 2006) proteins and is involved in ribosome synthesis and the p53 signalling cascade (Selinger et al., 2022).

The top-ranked TBEV C-interacting partners further revealed by the CO-IP included the proteins OASL and IFIT1. In the case of flaviviruses, both proteins are well-described antiviral effectors, and TBEV C may dysregulate the expression of host genes by interacting with these proteins (Selinger et al., 2022).

Unfortunately, none of these proteins were identified in this thesis, and the only matching proteins were: TBEV NS5, 60S ribosomal protein L23a (UniProt ID: K7EMA7, gene: RPL23A), and Alpha-enolase (UniProt ID: A0A2R8Y798, gene: ENO1), which have

already been identified as NS3/NS5 binding protein (le Breton et al., 2011); however, these two proteins were identified within the non-benzonase MEB fraction (Alpha-enolase also detected in the non-benzonase nuclear fraction), which could indicate that the interaction with these proteins is nucleic acid-mediated.
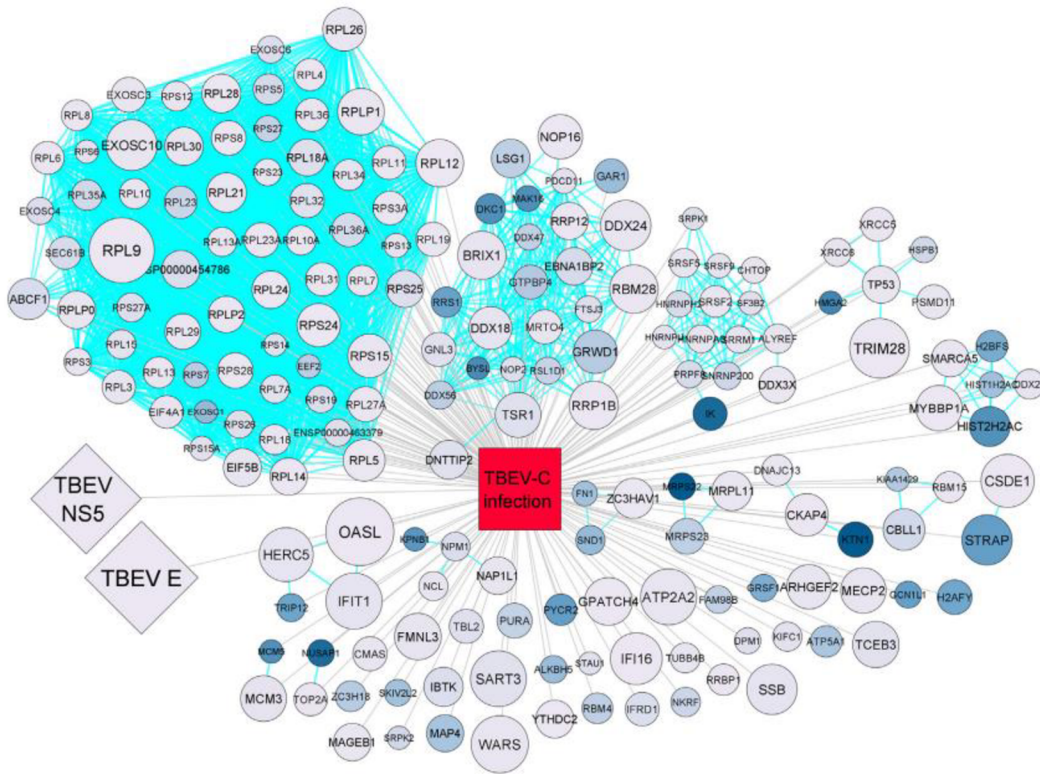

Figure 21: Whole-cell TBEV C interactome identified via TBEV C-specific CO-IP. DAOY cells were infected with TBEV Hypr (5 MOI) and lysed at 36 hpi. Lysates were used for TBEV C-specific CO-IP using anti-TBEV C antibodies and Dynabeads coupled with protein A. Proteins interacting with TBEV C were subsequently identified using LC–MS/MS. The interaction network (grey lines) combined with the STRING database (light blue lines), and statistical evaluation were generated in CytoScape software, version 3.8.2 (Selinger et al., 2022).

In this work, the TBEV C cytoplasmic, membrane, and nuclear interactomes were described. The most significant finding was the possible interaction of TBEV C with histones (H2A and H2B) and glycolytic enzymes (GAPDH, LDHA, and TKT). Despite intensive research, this work contains many facts that need to be further experimentally verified to better understand the function of TBEV C in the nucleus. In the future, it is proposed to focus again on SF and CO-IP optimization with the purpose of limiting the degree of contamination between fractions. It is also suggested to verify the obtained results (especially H2B MEB localization) using fluorescence microscopy or detection using WB.

7 Conclusion

In conclusion, this work provides insight into the possible functions of TBEV C through the identification of the cytoplasmic, membrane, and nuclear interactomes of this protein. It was found that TBEV C can target histones (H2A and H2B) and interact with the glycolytic enzymes GAPDH, LDHA, and TKT under stress conditions during the infection process.

Although the optimization experiments showed favourable results, the MS identification did not provide sufficiently relevant data for the overall evaluation. It was discovered that there was no significant difference between samples with and without benzonase, and only a small number of proteins were identified in at least 2 biological replicates. Therefore, further optimization and research are required to better understand the TBEV C protein and its functions.

8 List of abbreviations

APS	Ammonium Peroxodisulfate
BCA	bicinchoninic acid
BOFES	foetal bovine serum
BSL2	biosafety level 2
C	capsid protein
CEB	cytoplasmic extraction buffer
CER I	cytoplasmic extraction reagent I
CER II	cytoplasmic extraction reagent II
CNS	central neural system
CO-IP	co-immunoprecipitation
DAPI	4′,6-diamidino-2-phenylindole
DENV	dengue virus
DTT	dithiothreitol
E	envelope protein
ER	endoplasmic reticulum
FA	formic acid
FDR	false discovery rate
FSc USB	Faculty of Science of the University of South Bohemia in České Budějovice
F-T	fraction containing unbound proteins (flow-through)
GAPDH	Glyceraldehyde-3-phosphate dehydrogenase
HCC	hepatocellular carcinoma
HIST1H2BH	Histone H2B type 1-H
hpi	hours post infection
HPV	human papillomavirus
HRP	horseradish peroxidase
iBAQ	intensity based absolute quantification
JEV	Japanese encephalitis virus
KDM1/LSD1	lysine Specific Histone Demethylase 1
KFD	Kyasanur forest disease
KFDV	Kyasanur forest disease virus
LB	loading buffer
LDHA	Lactate dehydrogenase A

LFQ	label-free quantification
LIV	Louping-ill virus
M	membrane protein
MEB	membrane extraction buffer
MgPA	*Mycoplasma genitalium* protein of adhesion
MOCK	brain suspension from uninfected mice
MOI	multiplicity of infection
MS	mass spectrometry
NCR	non-coding regions
NEB	nuclear extraction buffer
NEB+	chromatin-bound extraction buffer
NER	nuclear extraction reagent
NLS	nuclear localization signal
NMR	nuclear magnetic resonance
OHFV	Omsk haemorrhagic fever virus
ORF	open reading frame
PBS	phosphate-buffered saline
PEB	pellet extraction buffer
POWV	Powassan virus
PPP	pentose phosphate pathway
prM	membrane protein glycosylated precursor
PSM	peptide spectrum match
PXMP4	Peroxisomal membrane protein 4
ROS	reactive oxygen species
SDS	sodium dodecyl sulfate
SDS-PAGE	SDS-polyacrylamide gel electrophoresis
SF	subcellular fractionation
SLC7A5	Large neutral amino acids transporter small subunit 1
SYPL1	Synaptophysin-like protein 1
TBE	tick-borne encephalitis
TBEV	tick-borne encephalitis virus
TBEV-Eu	European subtype
TBEV-FE	Far Eastern subtype
TBEV-Sib	Siberian subtype

TCE	2,2,2-trichloroethanol
TKT	Transketolase
TMED2	Transmembrane emp24 domain - containing protein 2
TUBB3	beta III-tubulin
VIM	vimentin
WNV	West Nile virus
ZIKV	Zika virus

9 References

Balinsky, C. A., Schmeisser, H., Ganesan, S., Singh, K., Pierson, T. C., & Zoon, K. C. (2013). **Nucleolin interacts with the dengue virus capsid protein and plays a role in formation of infectious virus particles.** *Journal of Virology*, *87*(24), 13094–13106. https://doi.org/10.1128/JVI.00704-13.

Barrows, N. J., Campos, R. K., Liao, K. C., Prasanth, K. R., Soto-Acosta, R., Yeh, S. C., Schott-Lerner, G., Pompon, J., Sessions, O. M., Bradrick, S. S., & Garcia-Blanco, M. A. (2018). **Biochemistry and molecular biology of flaviviruses.** *Chemical Reviews*, *118*(8), 4448–4482.

Bhatt, S., Gething, P. W., Brady, O. J., Messina, J. P., Farlow, A. W., Moyes, C. L., Drake, J. M., Brownstein, J. S., Hoen, A. G., Sankoh, O., Myers, M. F., George, D. B., Jaenisch, T., William Wint, G. R., Simmons, C. P., Scott, T. W., Farrar, J. J., & Hay, S. I. (2013). **The global distribution and burden of dengue.** *Nature*, *496*(7446), 504–507. https://doi.org/10.1038/nature12060.

Bhuvanakantham, R., & Ng, M. L. (2013). **West Nile virus and dengue virus capsid protein negates the antiviral activity of human Sec3 protein through the proteasome pathway.** *Cellular Microbiology*, *15*(10), 1688–1706.

Carvalho, F. A., Carneiro, F. A., Martins, I. C., Assunção-Miranda, I., Faustino, A. F., Pereira, R. M., Bozza, P. T., R B Castanho, M. A., Mohana-Borges, R., Da Poian, A. T., Santos, N. C., Oswaldo Cruz, I., Oswaldo Cruz, F., & de Janeiro, R. (2011). **Dengue virus capsid protein binding to hepatic lipid droplets (LD) is potassium ion dependent and is mediated by LD surface proteins.** *Journal of Virology*, *86*(4), 2096–2108. https://doi.org/10.1128/JVI.06796-11.

CDC, & DHCPP. (n.d.). **Tick-borne encephalitis (TBE).** *National Center for Emerging and Zoonotic Infectious Diseases Division of High-Consequence Pathogens and Pathology (DHCPP).*

Chambers, T. J., & Diamond, M. S. (2003). **Pathogenesis of flavivirus encephalitis.** *Advances in Virus Research*, *60*, 273–342.

Colpitts, T. M., Barthel, S., Wang, P., & Fikrig, E. (2011). **Dengue virus capsid protein binds core histones and inhibits nucleosome formation in human liver cells.** *PLoS ONE*, *6*(9). https://doi.org/10.1371/journal.pone.0024365.

Cox, J., & Mann, M. (2008). **MaxQuant enables high peptide identification rates, individualized p.p.b.-range mass accuracies and proteome-wide protein quantification.** *Nature Biotechnology, 26*(12), 1367–1372.

Dai, X., Shang, G., Lu, S., Yang, J., & Xu, J. (2018). **A new subtype of eastern tick-borne encephalitis virus discovered in Qinghai-Tibet Plateau, China article.** *Emerging Microbes and Infections*, *7*(1). https://doi.org/10.1038/s41426-018-0081-6.

Dobler, G. (2010). **Zoonotic tick-borne flaviviruses.** *Veterinary Microbiology*, *140*(3–4), 221–228. https://doi.org/10.1016/J.VETMIC.2009.08.024.

Dokland, T., Walsh, M., Mackenzie, J. M., Khromykh, A. A., Ee, K. H., & Wang, S. (2004). **West Nile virus core protein: Tetramer structure and ribbon formation.** *Structure, 12*(7), 1157. https://doi.org/10.1016/J.STR.2004.04.024.

Flaviviridae ~ ViralZone. (n.d.). Retrieved January 30, 2023, from https://viralzone.expasy.org/43?outline=all_by_species.

Folly, A. J., McElhinney, L. M., & Johnson, N. (2022). **JMM profile: Louping ill virus.** *Journal of Medical Microbiology*, *71*(5).

Fontaine, K. A., Leon, K. E., Khalid, M. M., Tomar, S., Jimenez-Morales, D., Dunlap, M., Kaye, J. A., Shah, P. S., Finkbeiner, S., Krogan, N. J., & Ott, M. (2018). **The cellular NMD pathway restricts Zika virus infection and is targeted by the viral capsid protein.** *MBio*, *9*(6). https://doi.org/10.1128/MBIO.02126-18.

Forinová, M., Pilipenco, A., Víšová, I., Lynn, N. S., Dostálek, J., Mašková, H., Hönig, V., Palus, M., Selinger, M., Kočová, P., Dyčka, F., Štěrba, J., Houska, M., Vrabcová, M., Horák, P., Anthi, J., Tung, C. P., Yu, C. M., Chen, C. Y., … Vaisocherová-Lísalová, H. (2021). **Functionalized terpolymer-brush-based biointerface with improved antifouling properties for ultra-sensitive direct detection of virus in crude clinical samples.** *ACS Applied Materials and Interfaces*, *13*(50), 60612–60624. https://doi.org/10.1021/ACSAMI.1C16930/SUPPL_FILE/AM1C16930_SI_003.XLS.

Gaunt, M. W., Sall, A. A., de Lamballerie, X., Falconar, A. K. I., Dzhivanian, T. I., & Gould, E. A. (2001). **Phylogenetic relationships of flaviviruses correlate with their epidemiology, disease association and biogeography.** *Journal of General Virology*, *82*(8), 1867–1876. https://doi.org/10.1099/0022-1317-82-8-1867/CITE/REFWORKS.

Geladaki, A., Britovšek, N. K., Breckels, L. M., Smith, T. S., Vennard, O. L., Mulvey, C. M., Crook, O. M., Gatto, L., & Lilley, K. S. (2019). **Combining LOPIT with differential ultracentrifugation for high-resolution spatial proteomics.**

Giard, D. J., Aaronson, S. A., Todaro, G. J., Arnstein, P., Kersey, J. H., Dosik, H., & Parks, W. P. (1973). *In vitro* **cultivation of human tumors: Establishment of cell lines derived from a series of solid tumors.** *JNCI: Journal of the National Cancer Institute*, *51*(5), 1417–1423. https://doi.org/10.1093/JNCI/51.5.1417.

Gould, E., & Solomon, T. (2008). **Pathogenic flaviviruses.** *The Lancet*, *371*(9611), 500–509. https://doi.org/10.1016/S0140-6736(08)60238-X.

Gritsun, T. S., Lashkevich, V. A., & Gould, E. A. (2003). **Tick-borne encephalitis.** *Antiviral Research*, *57*(1–2), 129–146. https://doi.org/10.1016/S0166-3542(02)00206-1.

Gubler, D. J. (1998). **Dengue and Dengue hemorrhagic fever.** *Clinical Microbiology Reviews*, *11*(3), 480. https://doi.org/10.1128/CMR.11.3.480.

Jacobsen, P. F., Jenkyn, D. J., & Papadimitriou, J. M. (1985). **Establishment of a human medulloblastoma cell line and its heterotransplantation into nude mice.** *Journal of Neuropathology & Experimental Neurology*, *44*(5), 472–485.

Jaklová, K. (2021). **Exprese proteinu NS5 viru klíšťové encefalitidy v lidských neurálních buňkách.** Bakalářská práce.

Jung, D. W., Kim, W. H., & Williams, D. R. (2014). **Chemical genetics and its application to moonlighting in glycolytic enzymes.** *Biochemical Society Transactions*, *42*(6), 1756–1761. https://doi.org/10.1042/BST20140201.

Kaufman, F., Dostálková, A., Pekárek, L., Thanh, T. D., Kapisheva, M., Hadravová, R., Bednárová, L., Novotný, R., Křížová, I., Černý, J., Grubhoffer, L., Ruml, T., Hrabal, R., & Rumlová, M. (2020). **Characterization and** *in vitro* **assembly of tick-borne encephalitis virus C protein.** *FEBS Letters*, *594*(12), 1989–2004. https://doi.org/10.1002/1873-3468.13857.

Kemenesi, G., & Bányai, K. (2019). **Tick-borne flaviviruses, with a focus on Powassan virus.** *Clinical Microbiology Reviews*, *32*(1). https://doi.org/10.1128/CMR.00106-17.

Kofler, R. M., Heinz, F. X., & Mandl, C. W. (2002). **Capsid protein C of tick-borne encephalitis virus tolerates large internal deletions and is a favorable target for attenuation of virulence.** *Journal of Virology*, *76*(7), 3534–3543. https://doi.org/10.1128/jvi.76.7.3534-3543.2002.

Kollaritsch, H., Paulke-Korinek, M., Holzmann, H., Hombach, J., Bjorvatn, B., & Barrett, A. (2012). **Vaccines and vaccination against tick-borne encephalitis.** *Expert Review of Vaccines*, *11*(9), 1103–1119. https://doi.org/10.1586/ERV.12.86.

Kovalev, S. Y., & Mukhacheva, T. A. (2017). **Reconsidering the classification of tick-borne encephalitis virus within the Siberian subtype gives new insights into its**

evolutionary history. *Infection, Genetics and Evolution*, *55*, 159–165. https://doi.org/10.1016/j.meegid.2017.09.014.

Kubinski, M., Beicht, J., Gerlach, T., Volz, A., Sutter, G., & Rimmelzwaan, G. F. (2020). **Tick-borne encephalitis virus: A quest for better vaccines against a virus on the rise.** *Vaccines 2020, Vol. 8, Page 451*, *8*(3), 451.

le Breton, M., Meyniel-Schicklin, L., Deloire, A., Coutard, B., Canard, B., de Lamballerie, X., Andre, P., Rabourdin-Combe, C., Lotteau, V., & Davoust, N. (2011). **Flavivirus NS3 and NS5 proteins interaction network: A high-throughput yeast two-hybrid screen.** *BMC Microbiology*, *11*. https://doi.org/10.1186/1471-2180-11-234.

Lee, Y. H., Tan, H. T., & Chung, M. C. M. (2010). **Subcellular fractionation methods and strategies for proteomics.** *PROTEOMICS*, *10*(22), 3935–3956.

Li, M., Johnson, J. R., Truong, B., Kim, G., Weinbren, N., Dittmar, M., Shah, P. S., Von Dollen, J., Newton, B. W., Jang, G. M., Krogan, N. J., Cherry, S., & Ramage, H. (2019). **Identification of antiviral roles for the exon-junction complex and nonsense-mediated decay in flaviviral infection.** *Nature Microbiology*, *4*(6), 985–995. https://doi.org/10.1038/S41564-019-0375-Z.

Liao, Y., Deng, X., Peng, K., Dai, P., Luo, D., Liu, P., Chen, L., Li, X., Ye, Y., & Zeng, Y. (2021). **Identification of histone H2B as a potential receptor for *Mycoplasma genitalium* protein of adhesion.** *Pathogens and disease*, *79*(7).

Lindqvist, R., Upadhyay, A., & Överby, A. K. (2018). **Tick-borne flaviviruses and the type I interferon response.** *Viruses*, *10*(7). https://doi.org/10.3390/v10070340.

Liu, Y., Guo, J.-Z., Liu, Y., Wang, K., Ding, W., Wang, H., Liu, X., Zhou, S., Lu, X.-C., Yang, H.-B., Xu, C., Gao, W., Zhou, L., Wang, Y.-P., Hu, W., Wei, Y., Huang, C., & Lei, Q.-Y. (2018). **Nuclear lactate dehydrogenase A senses ROS to produce α-hydroxybutyrate for HPV-induced cervical tumor growth.**

Ma, L., Jones, C. T., Groesch, T. D., Kuhn, R. J., & Post, C. B. (2004). **Solution structure of dengue virus capsid protein reveals another fold.** *Proceedings of the National Academy of Sciences of the United States of America*, *101*(10), 3414. https://doi.org/10.1073/PNAS.0305892101.

Mandl, C. W. (2005). **Steps of the tick-borne encephalitis virus replication cycle that affect neuropathogenesis.** *Virus Research*, *111*(2), 161–174.

Martins, A. S., Carvalho, F. A., Faustino, A. F., Martins, I. C., & Santos, N. C. (2019). **West Nile virus capsid protein interacts with biologically relevant host lipid systems.** *Frontiers in Cellular and Infection Microbiology*, *9*.

Mazeaud, C., Freppel, W., & Chatel-Chaix, L. (2018). **The multiples fates of the flavivirus RNA genome during pathogenesis.** *Frontiers in Genetics, 9.* Frontiers Media S.A. https://doi.org/10.3389/fgene.2018.00595.

Munivenkatappa, A., Sahay, R. R., Yadav, P. D., Viswanathan, R., & Mourya, D. T. (2018). **Clinical & epidemiological significance of Kyasanur forest disease.** *The Indian Journal of Medical Research*, *148*(2), 145. https://doi.org/10.4103/IJMR.IJMR_688_17.

Nabbi, A., & Riabowol, K. (2015). **Rapid Isolation of Nuclei from Cells** *In Vitro. Cold Spring Harbor Protocols*, 8, 769–772.

Orlíková, H., Lenz, P., Vlčková, I., & Kynčl, J. (2021). **Klíšťová encefalitida v České republice v roce 2020 [Tick-borne encephalitis in the Czech Republic in 2020],** *30.*

Pielnaa, P., Al-Saadawe, M., Saro, A., Dama, M. F., Zhou, M., Huang, Y., Huang, J., & Xia, Z. (2020). **Zika virus-spread, epidemiology, genome, transmission cycle, clinical manifestation, associated challenges, vaccine and antiviral drug development.** *Virology*, *543*, 34–42. https://doi.org/10.1016/J.VIROL.2020.01.015.

Plourde, A. R., & Bloch, E. M. (2016). **A literature review of Zika virus.** *Emerging Infectious Diseases*, *22*(7), 1185. https://doi.org/10.3201/EID2207.151990.

Product contents Dynabeads ® Protein A contains 30 mg Dynabeads ® /mL in phosphate. (n.d.). www.lifetechnologies.com/magnets.

Pulkkinen, L. I. A., Butcher, S. J., & Anastasina, M. (2018). **Tick-borne encephalitis virus: A structural view.** *Viruses*, *10*(7). https://doi.org/10.3390/v10070350.

Qin, Z., Xiang, C., Zhong, F., Liu, Y., Dong, Q., Li, K., Shi, W., Ding, C., Qin, L., & He, F. (2019). **Transketolase (TKT) activity and nuclear localization promote hepatocellular carcinoma in a metabolic and a non-metabolic manner.** *Journal of Experimental and Clinical Cancer Research*, *38*(1), 1–21.

Rappsilber, J., Mann, M., & Ishihama, Y. (2007). **Protocol for micro-purification, enrichment, pre-fractionation and storage of peptides for proteomics using StageTips.** *Nature Protocols, 2*(8), 1896–1906.

Roby, J. A., Setoh, Y. X., Hall, R. A., & Khromykh, A. A. (2015). **Post-translational regulation and modifications of flavivirus structural proteins.** *The Journal of General Virology*, *96*(7), 1551–1569. https://doi.org/10.1099/VIR.0.000097.

Salles, T. S., da Encarnação Sá-Guimarães, T., de Alvarenga, E. S. L., Guimarães-Ribeiro, V., de Meneses, M. D. F., de Castro-Salles, P. F., dos Santos, C. R., do Amaral Melo, A. C., Soares, M. R., Ferreira, D. F., & Moreira, M. F. (2018). **History, epidemiology**

and diagnostics of dengue in the American and Brazilian contexts: a review. *Parasites & Vectors*, *11*(1). https://doi.org/10.1186/S13071-018-2830-8.

Schneider, H. (1931). **Uber epidemische akute Meningitis serosa.** *Wiener klinische Wochenschrift, 44*. 350-352.

Selinger, M., Novotný, R., Sýs, J., Roby, J. A., Tykalová, H., Ranjani, G. S., Vancová, M., Jaklová, K., Kaufman, F., Bloom, M. E., Zdráhal, Z., Grubhoffer, L., Forwood, J. K., Hrabal, R., Rumlová, M., & Štěrba, J. (2022). **Tick-borne encephalitis virus capsid protein induces translational shutoff as revealed by its structural–biological analysis.** *Journal of Biological Chemistry*, *298*(11), 102585.

Sen, N., Hara, M. R., Kornberg, M. D., Cascio, M. B., Bae, B. Il, Shahani, N., Thomas, B., Dawson, T. M., Dawson, V. L., Snyder, S. H., & Sawa, A. (2008). **Nitric oxide-induced nuclear GAPDH activates p300/CBP and mediates apoptosis.** *Nature Cell Biology, 10*(7), 866–873. https://doi.org/10.1038/ncb1747.

Shechter, D., Dormann, H. L., Allis, C. D., & Hake, S. B. (2007). **Extraction, purification and analysis of histones.** *Nature Protocols*, *2*(6), 1445–1457.

Simmonds, P., Becher, P., Bukh, J., Gould, E. A., Meyers, G., Monath, T., Muerhoff, S., Pletnev, A., Rico-Hesse, R., Smith, D. B., & Stapleton, J. T. (2017). **ICTV virus taxonomy profile:** *Flaviviridae.* *Journal of General Virology*, *98*, 2–3. https://doi.org/10.1099/jgv.0.000672.

Sotcheff, S., & Routh, A. (2020). **Understanding flavivirus capsid protein functions: The tip of the iceberg.** *Pathogens, 9*(1), 42.

Stewart, N. A., & Veenstra, T. D. (2008). **Sample preparation for mass spectrometry analysis of formalin-fixed paraffin-embedded tissue: proteomic analysis of formalin-fixed tissue.** *Methods in molecular biology*, 425, 131–138. https://doi.org/10.1007/978-1-60327-210-0_11.

Tsuda, Y., Mori, Y., Abe, T., Yamashita, T., Okamoto, T., Ichimura, T., Moriishi, K., & Matsuura, Y. (2006). **Nucleolar protein B23 interacts with Japanese encephalitis virus core protein and participates in viral replication.** *Microbiology and Immunology*, *50*(3), 225–234. https://doi.org/10.1111/J.1348-0421.2006.TB03789.X.

Tyanova, S., & Cox, J. (2018). **Perseus: A bioinformatics platform for integrative analysis of proteomics data in cancer research.** *Methods in Molecular Biology*, *1711*, 133–148. https://doi.org/10.1007/978-1-4939-7493-1_7/FIGURES/5.

Valarcher, J. F., Hägglund, S., Juremalm, M., Blomqvist, G., Renström, L., Zohari, S., Leijon, M., & Chirico, J. (2015). **Tick-borne encephalitis.** *Rev. Sci. Tech. Off. Int. Epiz*, *34*(2), 453–466.

Xing, Y., Schmitt, H. J., Arguedas, A., & Yang, J. (2017). **Tick-borne encephalitis in China: A review of epidemiology and vaccines.** *Vaccine*, *35*(9), 1227–1237. https://doi.org/10.1016/J.VACCINE.2017.01.015.

Zhang, X., Zhang, Y., Jia, R., Wang, M., Yin, Z., & Cheng, A. (2021). **Structure and function of capsid protein in flavivirus infection and its applications in the development of vaccines and therapeutics.** *Veterinary research, 52*(1), 98.

10 Supplementary data

Table XIV: MS identification (1).

Table XV: MS identification (2).

Table XVI: MS identification (3).